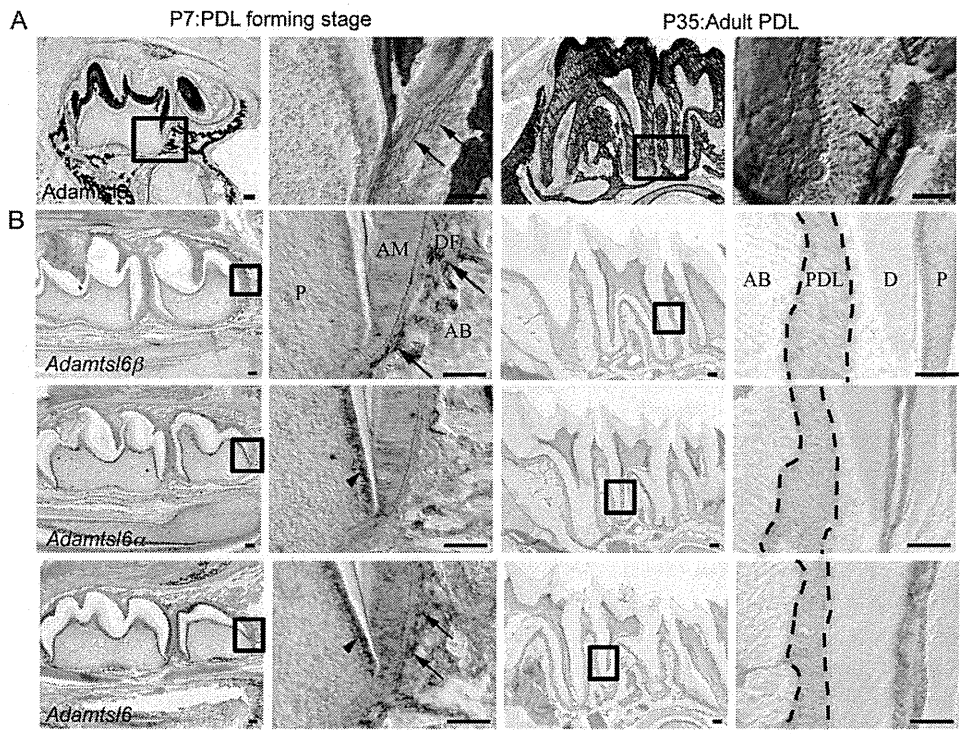

FIGURE 2. **Expression patterning of Adamtsl6α and -β during the PDL-forming stage.** *A*, sagittal sections of lower molar at P7 and P35 were immunostained with anti-Adamtsl6 antibody. The *image* in the *box* on the *left* is shown at higher magnification on the *right*. Note that Adamtsl6 protein was deposited as microfibril aggregates in DF at the PDL-forming stage (*arrows*) and formed a mature microfibrillar assembly in adult PDL (*arrows*). *Bar*, 100 μm. *B*, *in situ* hybridization analysis using a specific probe for *Adamtsl6α* and *-β* and control probe are shown. *Adamtsl6β* mRNA at the P1-late bell stage of dental follicle formation in the tooth germ is indicated by *arrows*. Expression of *Adamtsl6α* was detected in the odontoblast (*arrowheads*) by specific probes. In contrast, control probes that detected the conserved region of Adamtsl6 recognized both odontoblast (*arrowhead*) and DF (*arrows*). *Bar*, 100 μm. *AB*, alveolar bone; *AM*, ameloblast; *D*, dentin; *P*, pulp; *DF*, dental follicle; *PDL*, periodontal ligament.

inserted into collagen fibers known as Sharpey's fibers in the cementum matrix and alveolar bone, which resembles tendinous tissue (26, 31). *In situ* hybridization analysis revealed that *Adamtsl6β* is barely expressed in the DF, the origin of PDL formation in the surrounding tooth germ (supplemental Fig. S1*B*), but was very strongly expressed in the PDL-forming stage of the DF at P7 (Fig. 2*B*). However, *Adamtsl6β* expression was significantly down-regulated in the adult PDL at P35 (Fig. 2*B*). In contrast to *Adamtsl6β*, *Adamtsl6α* was found to be expressed in odontoblasts but not to be expressed in either the DF during the PDL-forming stage or in the adult PDL (supplemental Fig. S1*B* and Fig. 2*B*). Immunohistochemical analysis further revealed that Adamtsl6 is only weakly expressed in the early stage (bell stage) DF (supplemental Fig. S1*A*) but became detectable in assembled microfibril-like structures during the PDL-forming stage of the DF and in organized microfibrils in the adult PDL (Fig. 2*A*). Using confocal microscopy analysis, Adamtsl6 was observed to colocalize with fibrillin-1 to form immature microfibrillar-like structures at the PDL-forming stage of the DF, which were then observed as fully assembled mature microfibril structures in the adult PDL (Fig. 3*A*).

Using an Adamtsl6 antibody, positively stained fibers were observed in the adult PDL that were almost identical to those marked by aldehyde fuchsin staining and are indicative of microfibrils (supplemental Fig. S2). This suggested that Adamtsl6 was a component of microfibrils. Because developmental processes involve similar mechanisms to wound healing, we next determined whether Adamtsl6β is involved in PDL microfibril assembly during wound healing using a tooth replantation model (supplemental Fig. S3*A*) (30). Histochemical analysis revealed an injured PDL with an irregular architecture at 3 days after replantation, although gradual healing then occurred at between 7 and 14 days after replantation (Fig. 3*B* and supplemental Fig. S3*B*). During these processes, *Adamtsl6β* and fibrillin-1 mRNA expression were found to be clearly induced in the PDL at 3–7 days after replantation but to decrease again by 14 days after replantation (Fig. 3*B*).

Similar to these gene expression patterns, Adamtsl6- and fibrillin-1-positive microfibrillar-like structures resembling those seen in the DF during the PDL-forming stage were markedly increased in the damaged PDL at 3–7 days after replantation. These structures had evolved into mature microfibrils by 14 days after replantation (Fig. 3*C* and supplemental Fig. S3*B*). In contrast to these gene expression patterns, the expression of periostin, a PDL differentiation marker, was detected at 7 days after replantation (supplemental Fig. S3*C*). These data indicate that fibrillin-1 microfibril formation is induced in the early stages of both PDL development and wound healing and that Adamtsl6β is involved in these processes.

ADAMTSL6β Regulates PDL Formation through Fibrillin-1 Microfibril Assembly—We have recently developed a new three-dimensional single cell processing technique, the organ germ method, which can be used to generate bioengineered tooth germ reconstituted from E14.5 molar tooth germ-derived epithelial and mesenchymal cells (24). Utilizing this system, we developed a transgenic bioengineered tooth germ by overex-

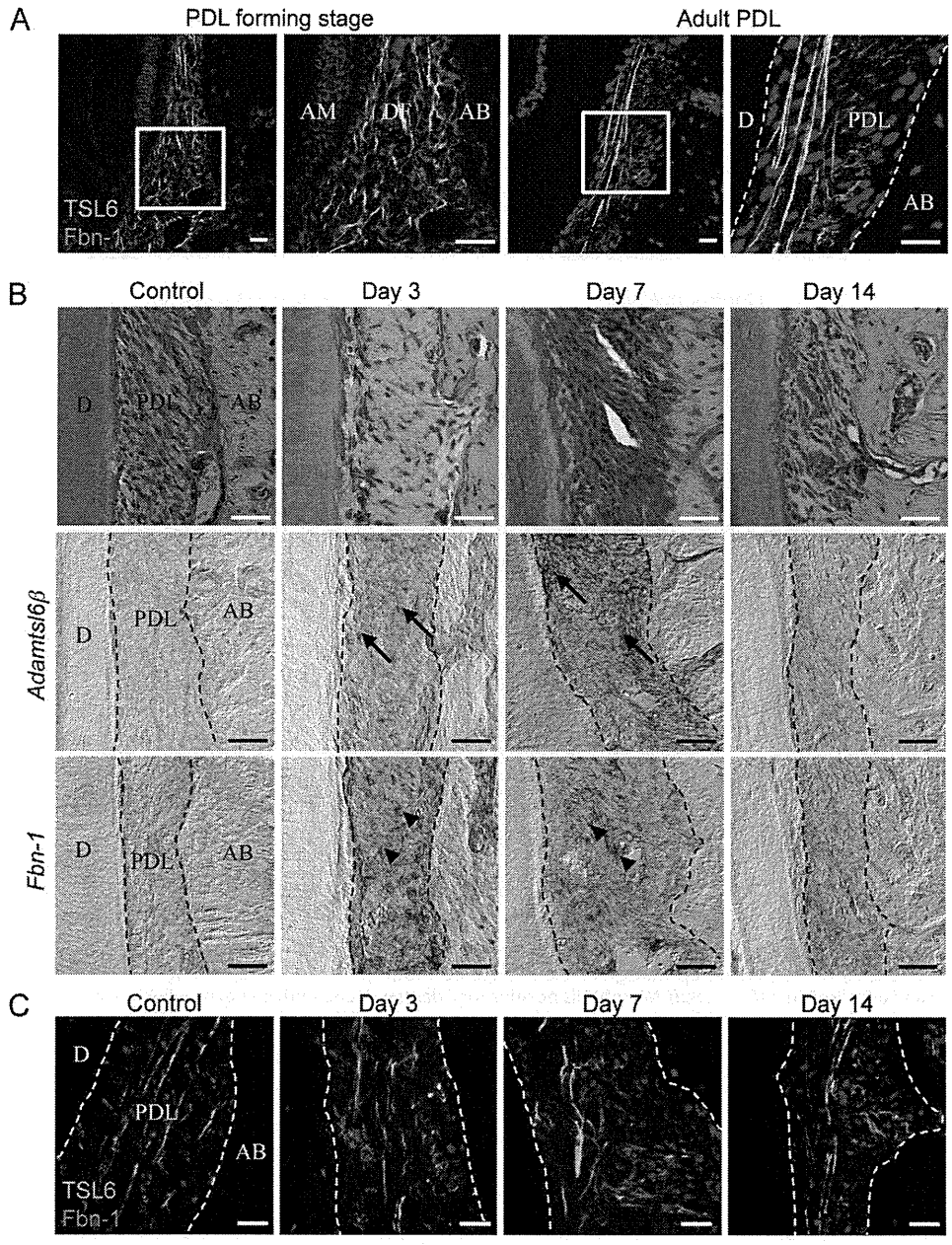

FIGURE 3. **Adamtsl6β is involved in fibrillin-1 microfibril formation during PDL development and wound healing.** *A*, localization of fibrillin-1- and Adamtsl6-positive microfibrils were analyzed during the PDL formation stage (*left*) and in adult PDL (*right*) using antibodies against Adamtsl6 (*TSL6; green*) and fibrillin-1 (*Fbn-1; red*). Formation of microfibrils positive for anti-Adamtsl6β and anti-fibrillin-1 was detectable during the process of PDL formation. *B*, frontal section of control side PDL and injured PDL 3, 7, and 14 days after replantation of the tooth were analyzed by hematoxylin and eosin staining (*top*) and *in situ* hybridization analysis of *Adamtsl6β* (*middle*) or fibrillin-1 (*Fbn-1; bottom*) expression in PDL. Cells positive for Adamtsl6β and fibrillin-1 mRNA expression are indicated by *arrows* or *arrowheads*, respectively. *C*, immunohistochemical analysis using anti-Adamtsl6 (*TSL6; green*) and anti-fibrillin-1 (*Fbn-1; red*) antibodies indicated that expression of Adamtsl6- and fibrillin-1-positive microfibrils was markedly increased 3 and 7 days after injury. A *merged image* illustrates that these fibrils were colocalized during the wound healing processes.

pressing exogenous genes in mesenchymal cells derived from tooth germ using adenovirus (supplemental Fig. S4, *A* and *B*). Because transgenic bioengineered tooth germ was found to accurately reproduce PDL development (supplemental Fig. S4, *C* and *D*), we generated *Adamtsl6β*-transgenic bioengineered tooth germ to examine the contributions of Adamtsl6β to PDL formation. Following immunohistochemical staining, *Adamtsl6β*-transgenic bioengineered tooth germs showed clear colocalization between fibrillin-1 microfibrils and Adamtsl6β (Fig. 4*A*) after 6 days of culture. Conversely, fibrillin-1 microfibrils were barely detectable in control *LacZ*-transgenic bioengineered tooth germ (Fig. 4*A*).

To confirm the role of Adamtsl6β in regulating microfibril formation in the DF from bioengineered tooth germ, we generated *Adamtsl6β* miRNAi-transgenic bioengineered tooth germ to suppress *Adamtsl6β* expression. Immunohistochemical analysis subsequently revealed that the *Adamtsl6β* miRNAi-transgenic germ exhibited poor Adamtsl6- and fibrillin-1-positive microfibril formation after 12 days of culture. However, no changes were observed in control miRNAi-transgenic bioengi-

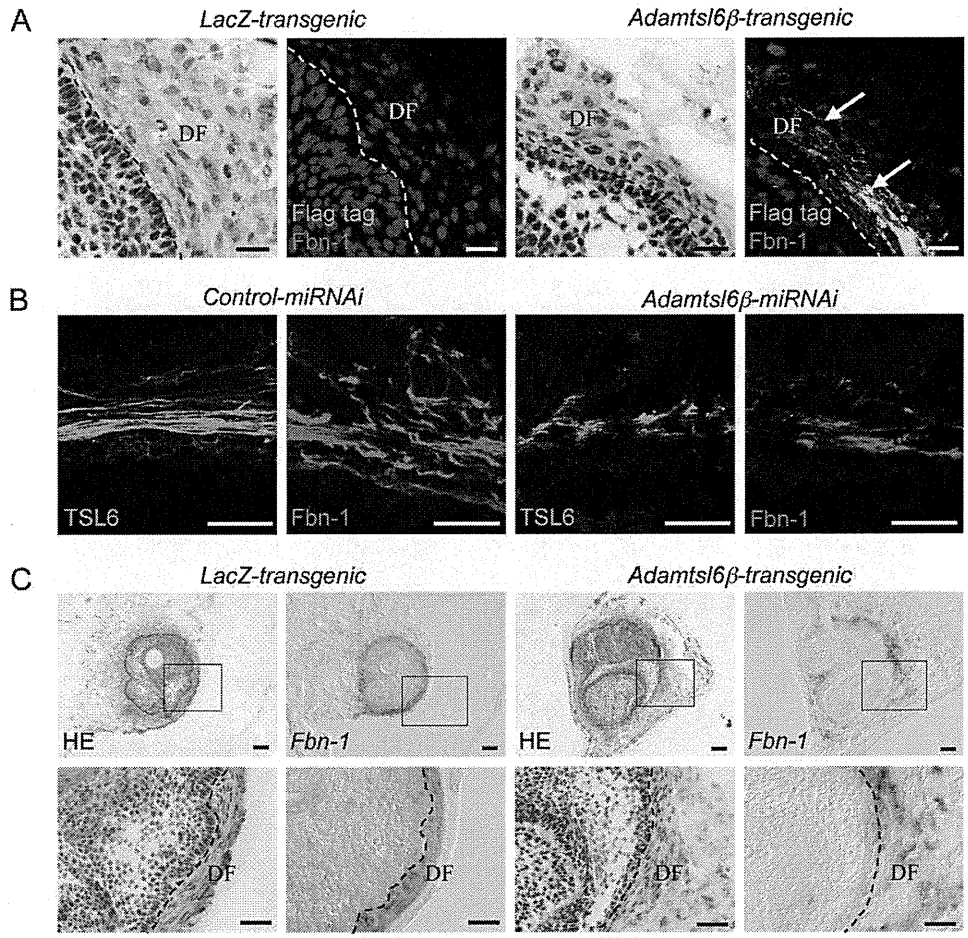

FIGURE 4. **Adamtsl6β contributes to PDL formation through regulation of fibrillin-1 microfibril assembly.** *A*, immunohistochemical analysis of *LacZ*-transgenic tooth germ (*LacZ-transgenic*) or *Adamtsl6β*-transgenic bioengineered tooth germ (*Adamtsl6β-transgenic*) using double immunostaining with anti-FLAG (*Flag tag; green*) and anti-fibrillin-1 (*Fbn-1; red*). Microfibrils positive for Adamtsl6β and fibrillin-1 expression are indicated by *arrows*. *B*, immunohistochemical analysis of control miRNAi-transgenic bioengineered tooth germ (*Control miRNAi*) or *Adamtsl6β* miRNAi-transgenic tooth germ (*Adamtsl6β-miRNAi*) using double immunostaining with anti-Adamtsl6 (*TSL6; green*) and anti-fibrillin-1 (*Fbn-1; red*). *C*, hematoxylin and eosin staining (*HE*) and *in situ* hybridization analysis of fibrillin-1 mRNA expression (*Fbn-1*) in *LacZ* transgenic tooth germ (*LacZ-transgenic*) or *Adamtsl6β* transgenic bioengineered tooth germ (*Adamtsl6β-transgenic*). The *image* in the *box* at the *top* is shown at higher magnification at the *bottom* (*C*).

neered tooth germ, further indicating that Adamtsl6β regulates microfibril assembly during PDL formation (Fig. 4*B*). We next evaluated whether the promotion of fibrillin-1 microfibril assembly was the result of increased mRNA expression. *In situ* hybridization analysis revealed that fibrillin-1 mRNA expression was similar in *LacZ*- and *Adamtsl6β*-transgenic bioengineered tooth germ (Fig. 4*C*). These data indicate that Adamtsl6β is capable of recruiting fibrillin-1 to assembling microfibrils without increasing the fibrillin-1 transcript levels.

ADAMTSL6β Negatively Regulates TGF-β-induced Periostin Gene Expression during PDL Formation—To investigate whether Adamtsl6β regulates PDL formation, we analyzed the expression of genes that function in PDL formation, including type I collagen, type XII collagen, periostin, and f-spondin (27). Among these genes, periostin, the protein product of which is known to be induced by TGF-β (32, 33), was markedly down-regulated in *Adamtsl6β*-transgenic bioengineered tooth germ (Fig. 5*B* and supplemental Fig. S5). *In situ* hybridization analysis further revealed the strong expression of periostin in the DF from *LacZ*-transgenic tooth germ when compared with the DF from *Adamtsl6β*-transgenic tooth germ (Fig. 5*A*). Real-time PCR analysis confirmed the suppression of periostin expression in *Adamtsl6β*-transgenic tooth germ (Fig. 5*B*).

To evaluate whether Adamtsl6β negatively regulates periostin gene expression in our MFS model system, we analyzed *Adamtsl6β* adenovirus-infected tooth germ obtained in MFS mice that were homozygous for a targeted hypomorphic allele (mgR/mgR) of fibrillin-1 (7). *In situ* hybridization analysis showed that periostin expression was remarkably reduced in developing tooth germ from mgR/mgR mice after infection with *Adamtsl6β*-adenovirus compared with *LacZ*-adenovirus-infected tooth germ (Fig. 5*C*). We next investigated the effects of ADAMTSL6β on human PDL cells obtained from an MFS patient with severe periodontitis (MHPDL) (25). As expected, *ADAMTSL6β* overexpression in these MHPDL cells clearly reduced periostin expression when compared with mock-infected cells. Interestingly, the level of periostin expression in MHPDL cells with *ADAMTSL6β* overexpression was comparable with that of normal HPDL cells (Fig. 5*D*), raising the possibility that ADAMTSL6β negatively regulates TGF-β and thereby reduces periostin expression. We evaluated this possibility by testing the ability of His-tagged recombinant Adamtsl6β to bind to TGF-β1. Interactions between

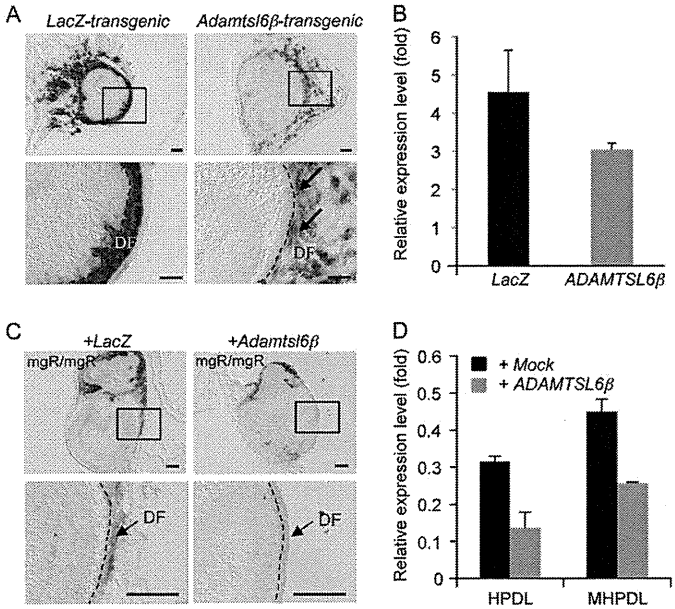

FIGURE 5. **ADAMTSL6β negatively regulates periostin expression.** *A, in situ* hybridization for periostin mRNA expression in *LacZ* transgenic tooth germ (*LacZ-transgenic*) or *Adamtsl6β* transgenic bioengineered tooth germ (*Adamtsl6β-transgenic*). The *image* in the *top box* is shown at higher magnification in the *bottom box*. Down-regulation of periostin mRNA expression in Adamtsl6β transgenic tooth germ is indicated by the *arrows*. *B*, total RNA extracted from *LacZ* (*LacZ*)- or Adamtsl6β (*Adamtsl6β*)-transgenic bioengineered tooth germ. cDNA was synthesized and subjected to quantitative real-time PCR for the expression of periostin and *GAPDH* transcripts. Levels of *GAPDH* transcript were used to normalize cDNA levels. Levels of *GAPDH* were set at 1, and relative expression levels are shown. Data are presented as triplicates, and the means ± S.D. are shown. *C, in situ* hybridization analysis of *Adamtsl6β*-adenovirus-infected mgR/mgR mouse tooth germ showed reduced periostin expression when compared with *LacZ*-adenovirus-infected mgR/mgR mouse tooth germ. *Bar*, 100 μm. *D*, real-time PCR analysis of periostin mRNA in HDPL and MHPDL cells transduced with mock or *Adamtsl6β*. Periostin mRNA expression was down-regulated in HPDL and MHPDL cells overexpressing *Adamtsl6β* as compared with expression in mock-overexpressed HPDL and MHPDL cells.

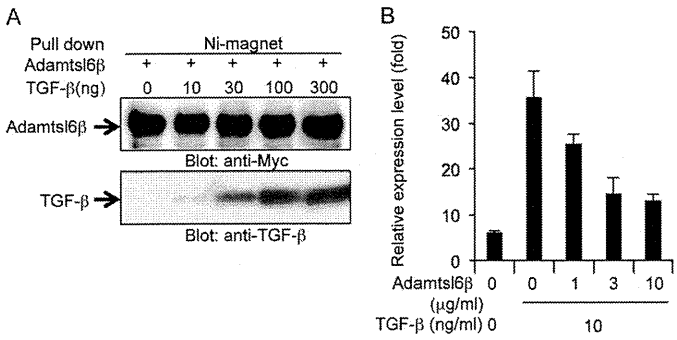

FIGURE 6. **Adamtsl6β binds TGF-β to negatively regulate periotsin gene expression.** *A*, His tag recombinant Adamtsl6β was incubated with TGF-β1 at the indicated concentrations followed by treatment with nickel-magnetic beads. Co-precipitates were detected using the corresponding antibodies, and Adamtsl6β was found to bind to TGF-β1 directly. *B*, mouse dental follicle cells were cultured with TGF-β1 for 3 days in the presence of recombinant mouse Adamtsl6β. Periostin mRNA levels were quantified by real-time PCR analysis. Adamtsl6β inhibited expression of periostin in a dose-dependent manner. *Error bars*, S.D.

Adamtsl6β and TGFβ1 were barely detectable at the 10 ng/ml concentrations, but strong associations between these proteins could be detected in a dose-dependent manner at 30, 100, or 300 ng/ml by pull-down analysis using nickel-magnetic beads (Fig. 6*A*). To then test the effects of recombinant Adamtsl6β on TGF-β activity, we measured the periostin expression levels in mouse dental follicle cells treated with Adamtsl6β in the presence or absence of TGF-β1. Recombinant Adamtsl6β inhibited TGF-β-induced periostin expression in a dose-dependent manner (Fig. 6*B*). These data suggest that Adamtsl6β directly binds to TGF-β to reduce periostin expression during the PDL-forming stage in both normal and MFS model settings.

The Local Administration of ADAMTSL6β Improves Wound Healing Ability in an MFS Model—We next investigated whether ADAMTSL6β alleviates fibrillin-1 microfibril disorder in MHPDL cells, which exhibit reduction in fibrillin-1 microfibril assembly (Fig. 7). The overexpression of *ADAMTSL6β* strongly induced fibrillin-1 microfibril assembly in MHPDL cells compared with the mock-infected controls (Fig. 7, *top* and *middle*). *Merged images* revealed that ADAMTSL6β colocalizes with fibrillin-1 in MHPDL cells that overexpress *ADAMTSL6β* (Fig. 7, *bottom*). We have previously shown that recombinant Adamtsl6β induces fibrillin-1 microfibril assembly in MG63 cells (17). Thus, we next investigated whether recombinant Adamtsl6β improves the symptoms of MHPDL microfibril disorder. We found that recombinant Adamtsl6β induces fibrillin-1 microfibril assembly in a dose-dependent manner in MHPDL cells during a 3-day incubation in culture (Fig. 8, *top* and *middle*). Staining with an anti-Adamtsl6 polyclonal antibody indicated that exogenous Adamtsl6 colocalizes with fibrillin-1 (Fig. 8, *bottom*). Endogenous fibrillin-1 was only marginally detectable in MHPDL cells. However, an abundant fibrillin-1 network formation was evident in the presence of high concentrations (10 μg/ml) of recombinant Adamtsl6β (Fig. 8, *top*). These results indicate that Adamtsl6β improved fibrillin-1 MHPDL microfibril assembly.

To investigate whether Adamtsl6β was capable of improving microfibril assembly *in vivo*, we investigated the PDL from mgR/mgR mice and by histochemical analysis observed a disorganized structure with a disrupted cell alignment, both of which are characteristic MFS morphologies (Fig. 9*A*). Immunohistochemical analysis clearly revealed fragmented Adamtsl6β- and fibrillin-1-positive microfibrils when compared with wild type mice (Fig. 9*A*, *arrows*). We next infected *Adamtsl6β* adenovirus into the DF of developing tooth germ isolated from mgR/mgR mouse embryos at E14.5 to evaluate the improvements in fibrillin-1 microfibril disorder during PDL formation. By histochemical analysis, we found that the overexpression of *Adamtsl6β* resulted in an improved DF morphology with compact and aligned cells (Fig. 9*B*). DF tooth germ infected with *LacZ* showed low cell numbers and an irregular architecture. Immunohistochemical analysis subsequently revealed that *Adamtsl6β* overexpression strongly induces fibrillin-1 microfibril assembly in the tooth germ from mgR/mgR mice, whereas no assembly was observed in *LacZ*-infected tooth germ (Fig. 9*B*, *arrows*). These data indicate that Adamtsl6β can indeed restore the impaired microfibrils in mgR/mgR mice.

We next investigated whether Adamtsl6β might be developed as a novel therapeutic for MFS microfibril disorder. Collagen gel containing recombinant Adamtsl6β was locally administrated into an experimentally damaged PDL in mgR/

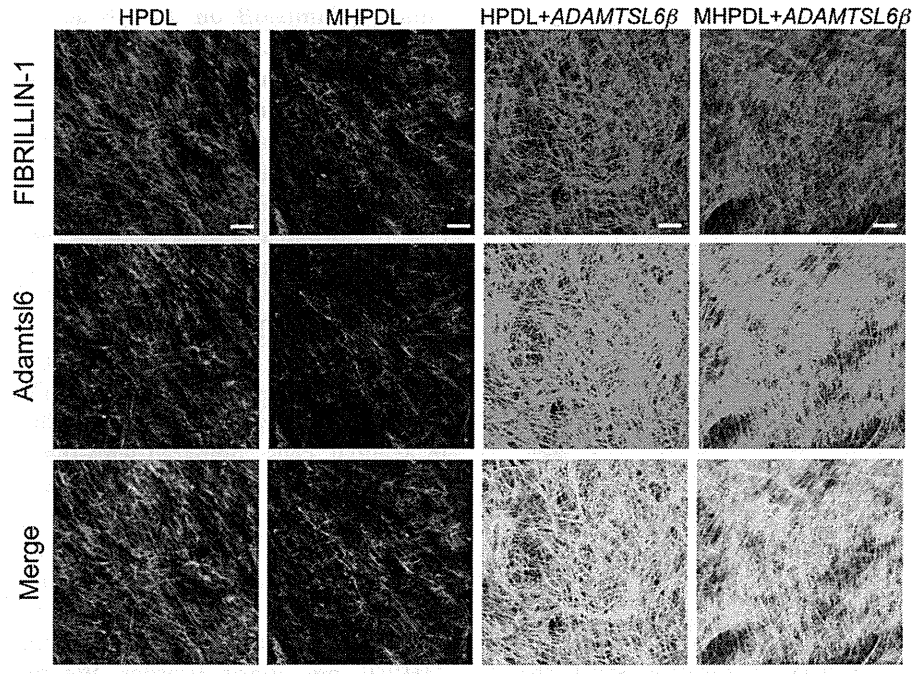

FIGURE 7. **Overexpression of *ADAMTSL6β* improves microfibril disorder in PDL from an MFS patient.** Immunohistochemical analysis of HPDL or MHPDL cells transduced with mock or *ADAMTSL6β* using anti-fibrillin-1 (*top*) and anti-ADAMTSL6 (*middle*) antibodies. The data show that ADAMTSL6β induces fibrillin-1 microfibril assembly in MHPDL cells. The *bottom images* were produced by superimposition of the *upper* and *middle images*, together with DAPI nuclear staining.

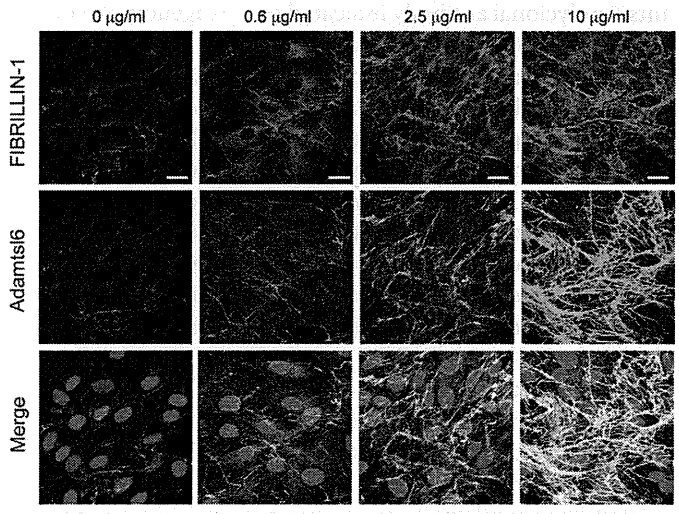

FIGURE 8. **Recombinant Adamtsl6β improves microfibril disorder in PDL from MFS patients.** Immunohistochemical analysis with anti-fibrillin-1 (*top*) and anti-Adamtsl6 (*middle*) antibodies reveals a marked improvement in fibrillin-1 microfibril assembly (*arrows*) in MHPDL cells incubated with purified recombinant Adamtsl6β at 0.6, 2.5, and 10 μg/ml for 3 days. The *bottom images* were produced by superimposition of the *upper* and *middle images*, together with DAPI nuclear staining.

mgR mice (supplemental Fig. S6, *A* and *B*). Fluorescence microscopic analysis revealed that the collagen gel implanted in damaged PDL was still present at 17 days after injection (supplemental Fig. S6*C*). Histochemical analysis showed that a damaged PDL could still be observed at 7 days after injection of the collagen gel containing recombinant Adamtsl6β (supplemental Fig. S6*D*). However, healing and improved cell alignment were apparent in the PDL of wild type mice at 17 days after injection (Fig. 9*C*, *asterisk*). Immunohistochemical analysis further revealed that the reorganization of fibrillin-1- and Adamtsl6-positive microfibril assembly could be observed after 17 days of incubation (Fig. 9*C* (*arrowheads*) and supplemental Fig. S6*E*). In contrast, the administration of control collagen gel failed to induce PDL healing, and an irregular cell morphology and poor fibrillin-1 microfibril formation could still be observed (Fig. 9*C* and supplemental Fig. S6*E*).

The enhanced activation of TGF-β has been suggested to directly contribute to tissue destruction in MFS (12). Ligand-activated TGF-β receptors induce the phosphorylation of Smad2 and Smad3 (pSmad2/3), which form a heteromeric complex with Smad4 that translocates to the nucleus and mediates the expression of target genes (34). The nuclear accumulation of pSmad2/3 has been detected in affected tissues in an MFS mouse model, including the aorta and skeletal muscle (10, 35). Consistent with these results, we observed the nuclear accumulation of pSmad2/3 in PDL from mgR/mgR mice 17 days after injection of control collagen gel in our current experiments (Fig. 9*D*). However, the local administration of Adamtsl6β markedly suppressed the nuclear localization of pSmad2/3. Further evidence for the Adamtsl6β suppression of TGF-β signaling is derived from the previous analysis of matrix metalloprotease (MMP)-9, which is known to be induced by TGF-β and is expressed in abnormal smooth muscle cells in the early vascular lesions that contribute to elastolysis (36, 37). In contrast to control collagen gel administration, the expression of MMP-9 was markedly suppressed by the administration of collagen gel containing recombinant Adamtsl6β (Fig. 9*D*). These results illustrate that reorganization of microfibrils by recombinant Adamtsl6β prevents the pathological activation of TGF-β by structurally damaged fibrillin-1 in MFS.

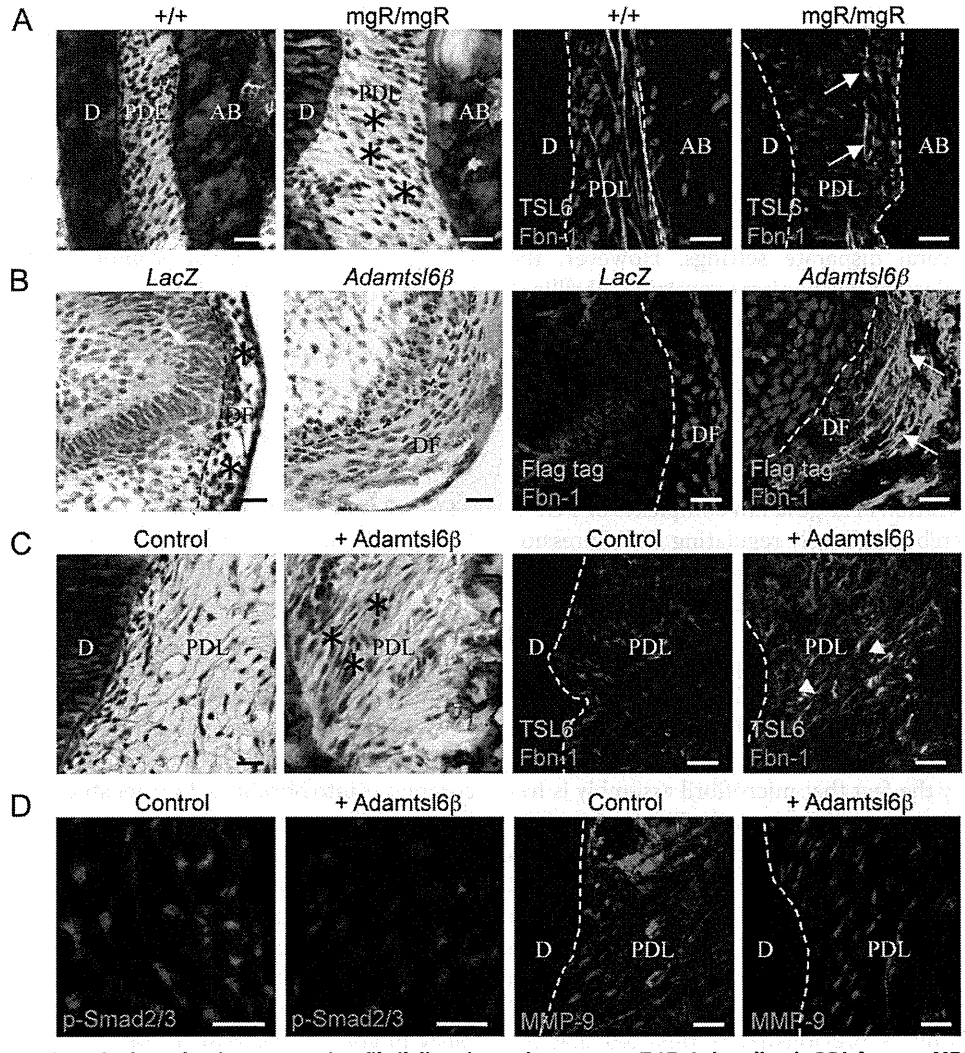

FIGURE 9. **Local administration of Adamtsl6β improves microfibril disorder and attenuates TGF-β signaling in PDL from an MFS model.** *A*, hematoxylin and eosin staining of a PDL revealing a markedly abnormal architecture in mgR/mgR mice when compared with wild type. Notable is the loosening of the PDL with an irregular cell alignment and an expanded cell-cell distance (*asterisks*). Immunohistochemical analysis using Adamtsl6 (*TSL6; green*) and fibrillin-1 (*Fbn-1; red*) antibodies revealed a clear disruption of fibrillin-1- and Adamtsl6-positive microfibrils in the PDL from mgR/mgR mice (*arrows*). *B*, hematoxylin and eosin staining of *LacZ*-infected mgR/mgR mouse tooth germ (*LacZ*) revealing an abnormal architecture with an irregular cell alignment (*asterisks*) when compared with *Adamtsl6β*-infected mgR/mgR mouse tooth germ (*Adamtsl6β*). Immunohistochemical analysis using FLAG (*Flag-tag; green*) and fibrillin-1 (*Fbn-1; red*) antibodies showed an improvement in fibrillin-1 microfibril assembly in *Adamtsl6β*-infected mgR/mgR mouse tooth germ (*arrows*). *C*, histological analysis of the injured PDL in mgR/mgR mice after the local administration of control gel or gel containing recombinant Adamtsl6β for 17 days. Hematoxylin and eosin staining revealed PDL healing after the injection of gel containing recombinant Adamtsl6β (*asterisks*) compared with the control. Immunohistochemical analysis further showed an improvement in fibrillin-1 microfibril assembly (*arrowheads*) induced by the injection of recombinant Adamtsl6β. *D*, immunohistochemical analysis of pSmad2/3 and MMP-9 expression in the injured PDL of mgR/mgR mice after the local administration of control gel or gel containing recombinant Adamtsl6β for 17 days. The suppression of nuclear accumulation of pSmad2/3 and MMP-9 expression is evident after injection of recombinant Adamtsl6β compared with the control gel.

DISCUSSION

Our current experiments successfully demonstrate that ADAMTSL6β has an essential role in PDL development and regeneration through the promotion of fibrillin-1 assembly and the negative regulation of TGF-β signaling. We also demonstrate in our present analyses that the local administration of ADAMTSL6β can rescue the disease manifestations of MFS in a mouse model, raising the possibility that this extracellular matrix protein could be used as a novel therapeutic agent for the treatment of MFS. Hence, our data show for the first time that the restoration of properly formed microfibrils by ADAMTSL6β is essential not only for improvement of the predominant symptoms of MFS but also for the suppression of excessive TGF-β signaling induced by microfibril disassembly.

To clarify the role of ADAMTSL6β in PDL formation, experiments were performed to determine whether ADAMTSL6β-mediated fibrillin-1 microfibril assembly is critical for PDL development and regeneration. The formation of fibrillin-1 microfibril networks has been shown to be essential for the development and growth of individual organ systems (38). Vascular smooth muscle cells are gradually organized via the formation of elastic fibers and interconnecting fibrillin-1 microfibrils during aortic media generation, resulting in the organization of elastic lamellae as the main determinant of arterial function (39). In addition to providing mechanical stability, previous studies have demonstrated that the organization of fibrillin-1 microfibril assemblies contributes to the regulation of the activities of signaling molecules, such as TGF-β and

BMP-7 (40, 41). During digit formation, fibrillin-1 may be a positive regulator that dictates the functional sites for cytokine concentration. In other tissues, fibrillin-1 acts as a negative regulator of signaling through cytokine sequestration (2, 7). Thus, the importance of microfibril network formation has been demonstrated in several disparate settings. However, the importance of the molecular mechanisms governing fibrillin-1 assembly during organogenesis has been hampered by the unanswered issue of the actual factor that drives microfibril assembly. Our present study demonstrates that ADAMTSL6β, an inducing factor for microfibril assembly (18), regulates development and regeneration of PDL. Furthermore, ADAMTSL6β-mediated fibrillin-1 microfibril assembly may accelerate the sequestration of large latent complexes of TGF-β or active TGF-β, thereby negatively regulating the expression of TGF-β regulatory targets, such as periostin (35, 42). Hence, our data provide significant insight into the molecular mechanisms by which ADAMTSL6β controls fibrillin-1 microfibril assembly and TGF-β signaling during organogenesis.

The establishment of fibrillin-1 microfibril assembly mechanisms is ultimately critical for the development of new MFS therapeutic approaches (12). The pathogenetic relevance of MFS is highlighted by the fact that microfibril assembly is frequently disrupted in patients with various fibrillinopathies (43). MFS fibrillinopathies have been explained by the structural insufficiency of fibrillin-1 microfibrils, leading to activation of TGF-β and its regulatory targets (7, 44). Although many recent publications have addressed the organization of fibrillins in microfibrils (45–48), relatively little information has been available regarding the mechanisms and components involved in microfibril formation. A previous study reported that the transgenic expression of wild-type fibrillin-1 alleles in a missense mutation (C1039G) heterozygous mouse model of MFS effectively rescues the aortic phenotype (11). From these data, essential improvements in fibrillin-1 microfibril formation represent a productive therapeutic strategy for the reduction of MFS disease severity (3).

In contrast to our present findings, another recent study has indicated that fibronectin is an essential component in the assembly of fibrillin-1 through its interaction with the C-terminal region of fibrillin-1, thus suggesting the possibility of improved microfibril assembly through regulation of fibrillin-1-associated proteins (49, 50). Our present data demonstrate, however, that the exogenous application of recombinant ADAMTSL6β improves fibrillin-1 microfibril assembly in an MFS mouse model. Hence, ADAMTSL6β reinforcement of fibrillin-1 microfibrils may represent a new, viable treatment for MFS. Although the mechanisms by which ADAMTSL6β accelerated fibrillin-1 microfibril assembly remain to be determined, in another study using the MFS mouse model and MHPDL cells, which are PDL cells obtained from an MFS patient, ADAMTSL6β seems to recruit available normal fibrillin-1 molecules and induce microfibril assembly with a resulting improvement in microfibril mechanical stability. These findings indicate that ADAMTSL6β is capable of enhancing microfibrils even in animals with a fibrillin-1 haploinsufficiency. Thus, ADAMTSL6β is potentially a novel therapeutic target for the treatment of MFS.

Recent evidence has suggested that restoration of microfibril assembly plays an important role in the prevention of pathological activation of TGF-β signaling in MFS (12). TGF-β is secreted from cells as a large latent complex consisting of TGF-β, latency-associated peptide, and LTBP-1 to be sequestered by fibrillin-1 (51). The promotion of fibrillin-1 microfibril assembly is therefore critical for the prevention of tissue destruction mediated by abnormal TGF-β signaling in MFS. In the present study, we have demonstrated that the reinforcement of fibrillin-1 microfibril assembly and the inhibition of TGFβ1 function by ADAMTSL6β facilitate wound healing in the PDL of mgR/mgR mice.

In conclusion, we provide evidence for the contributions of ADAMTSL6β-mediated fibrillin-1 microfibril assembly to PDL development, regeneration, and alleviation of MFS manifestations. We thereby introduce the concept that a fibrillin-1-associated protein, such as ADAMTSL6β, which induces microfibril assembly, should be considered in the development of future mechanism-based therapeutics for the improvement of connective tissue disorders, such as MFS. Our data suggest that the reinforcement of fibrillin-1 assembly by ADAMTSL6β accelerates the sequestration of newly synthesized large latent complexes into fibrillin-1. Further studies will help to clarify the nature of the interactions between ADAMTSL6β, fibrillin-1, TGF-β, and LTBP-1 and reveal how ADAMTSL6β expression suppresses TGF-β signaling. It will also be necessary to develop methodologies for the systemic administration of ADAMTSL6β to induce fibrillin-1 microfibril assembly in connective tissue for the treatment of life-threatening conditions, such as aortic aneurysm. Because elastolysis occurs continuously in aortic aneurysms in MFS, chronic administration of ADAMTSL6β may be required for the stabilization of microfibrils to prevent progressive tissue destruction. This approach will facilitate drug discovery for treating MFS and related connective tissue disorders.

Acknowledgments—We thank Dr. Lynn Sakai for providing the anti-fibrillin-1 polyclonal antibody (pAb9543) and Dr. Francesco Ramirez for providing the mgR/mgR mice. We also thank Drs. Zenzo Isogai, Takamasa Yokoi, Momotoshi Shiga, Tomoko Wada, and Hayato Ohshima for valuable advice and discussions during the course of this work.

REFERENCES

1. Straub, A. M., Grahame, R., Scully, C., and Tonetti, M. S. (2002) *J. Periodontol.* **73,** 823–826
2. Ramirez, F., and Dietz, H. C. (2007) *J. Cell Physiol.* **213,** 326–330
3. Judge, D. P., and Dietz, H. C. (2005) *Lancet* **366,** 1965–1976
4. Dietz, H. C., Loeys, B., Carta, L., and Ramirez, F. (2005) *Am. J. Med. Genet. C Semin. Med. Genet.* **139,** 4–9
5. Sakai, L. Y., Keene, D. R., and Engvall, E. (1986) *J. Cell Biol.* **103,** 2499–2509
6. Ramirez, F., and Dietz, H. C. (2007) *Curr. Opin. Genet. Dev.* **17,** 252–258
7. Pereira, L., Lee, S. Y., Gayraud, B., Andrikopoulos, K., Shapiro, S. D., Bunton, T., Biery, N. J., Dietz, H. C., Sakai, L. Y., and Ramirez, F. (1999) *Proc. Natl. Acad. Sci. U.S.A.* **96,** 3819–3823
8. Neptune, E. R., Frischmeyer, P. A., Arking, D. E., Myers, L., Bunton, T. E., Gayraud, B., Ramirez, F., Sakai, L. Y., and Dietz, H. C. (2003) *Nat. Genet.* **33,** 407–411
9. Carta, L., Pereira, L., Arteaga-Solis, E., Lee-Arteaga, S. Y., Lenart, B.,

Starcher, B., Merkel, C. A., Sukoyan, M., Kerkis, A., Hazeki, N., Keene, D. R., Sakai, L. Y., and Ramirez, F. (2006) *J. Biol. Chem.* **281,** 8016–8023
10. Habashi, J. P., Judge, D. P., Holm, T. M., Cohn, R. D., Loeys, B. L., Cooper, T. K., Myers, L., Klein, E. C., Liu, G., Calvi, C., Podowski, M., Neptune, E. R., Halushka, M. K., Bedja, D., Gabrielson, K., Rifkin, D. B., Carta, L., Ramirez, F., Huso, D. L., and Dietz, H. C. (2006) *Science* **312,** 117–121
11. Judge, D. P., Biery, N. J., Keene, D. R., Geubtner, J., Myers, L., Huso, D. L., Sakai, L. Y., and Dietz, H. C. (2004) *J. Clin. Invest.* **114,** 172–181
12. Judge, D. P., and Dietz, H. C. (2008) *Annu. Rev. Med.* **59,** 43–59
13. Ng, C. M., Cheng, A., Myers, L. A., Martinez-Murillo, F., Jie, C., Bedja, D., Gabrielson, K. L., Hausladen, J. M., Mecham, R. P., Judge, D. P., and Dietz, H. C. (2004) *J. Clin. Invest.* **114,** 1586–1592
14. Hirohata, S., Wang, L. W., Miyagi, M., Yan, L., Seldin, M. F., Keene, D. R., Crabb, J. W., and Apte, S. S. (2002) *J. Biol. Chem.* **277,** 12182–12189
15. Le Goff, C., Morice-Picard, F., Dagoneau, N., Wang, L. W., Perrot, C., Crow, Y. J., Bauer, F., Flori, E., Prost-Squarcioni, C., Krakow, D., Ge, G., Greenspan, D. S., Bonnet, D., Le Merrer, M., Munnich, A., Apte, S. S., and Cormier-Daire, V. (2008) *Nat. Genet.* **40,** 1119–1123
16. Ahram, D., Sato, T. S., Kohilan, A., Tayeh, M., Chen, S., Leal, S., Al-Salem, M., and El-Shanti, H. (2009) *Am. J. Hum. Genet.* **84,** 274–278
17. Tsutsui, K., Manabe, R., Yamada, T., Nakano, I., Oguri, Y., Keene, D. R., Sengle, G., Sakai, L. Y., and Sekiguchi, K. (2010) *J. Biol. Chem.* **285,** 4870–4882
18. Sawada, T., Sugawara, Y., Asai, T., Aida, N., Yanagisawa, T., Ohta, K., and Inoue, S. (2006) *J. Histochem. Cytochem.* **54,** 1095–1103
19. Tsuruga, E., Irie, K., and Yajima, T. (2002) *J. Dent. Res.* **81,** 771–775
20. Staszyk, C., and Gasse, H. (2004) *Anat. Histol. Embryol.* **33,** 17–22
21. Kawamoto, T. (1990) *J. Histochem. Cytochem.* **38,** 1805–1814
22. Nishimura, R., Hata, K., Harris, S. E., Ikeda, F., and Yoneda, T. (2002) *Bone* **31,** 303–312
23. Yamamoto, T., Miyoshi, H., Yamamoto, N., Yamamoto, N., Inoue, J., and Tsunetsugu-Yokota, Y. (2006) *Blood* **108,** 3305–3312
24. Nakao, K., Morita, R., Saji, Y., Ishida, K., Tomita, Y., Ogawa, M., Saitoh, M., Tomooka, Y., and Tsuji, T. (2007) *Nat. Methods* **4,** 227–230
25. Shiga, M., Saito, M., Hattori, M., Torii, C., Kosaki, K., Kiyono, T., and Suda, N. (2008) *Cell Tissue Res.* **331,** 461–472
26. Handa, K., Saito, M., Yamauchi, M., Kiyono, T., Sato, S., Teranaka, T., and Sampath Narayanan, A. (2002) *Bone* **31,** 606–611
27. Nishida, E., Sasaki, T., Ishikawa, S. K., Kosaka, K., Aino, M., Noguchi, T., Teranaka, T., Shimizu, N., and Saito, M. (2007) *Gene* **404,** 70–79
28. Nakajima, M., Kizawa, H., Saitoh, M., Kou, I., Miyazono, K., and Ikegawa, S. (2007) *J. Biol. Chem.* **282,** 32185–32192
29. Yokoi, T., Saito, M., Kiyono, T., Iseki, S., Kosaka, K., Nishida, E., Tsubakimoto, T., Harada, H., Eto, K., Noguchi, T., and Teranaka, T. (2007) *Cell Tissue Res.* **327,** 301–311
30. Hasegawa, T., Suzuki, H., Yoshie, H., and Ohshima, H. (2007) *Cell Tissue Res.* **329,** 259–272
31. Nanci, A., and Bosshardt, D. D. (2006) *Periodontol 2000* **40,** 11–28
32. Goetsch, S. C., Hawke, T. J., Gallardo, T. D., Richardson, J. A., and Garry, D. J. (2003) *Physiol. Genomics* **14,** 261–271
33. Cheng, J., and Grande, J. P. (2002) *Exp. Biol. Med.* **227,** 943–956
34. Heldin, C. H., Miyazono, K., and ten Dijke, P. (1997) *Nature* **390,** 465–471
35. Cohn, R. D., van Erp, C., Habashi, J. P., Soleimani, A. A., Klein, E. C., Lisi, M. T., Gamradt, M., ap Rhys, C. M., Holm, T. M., Loeys, B. L., Ramirez, F., Judge, D. P., Ward, C. W., and Dietz, H. C. (2007) *Nat. Med.* **13,** 204–210
36. Chou, Y. T., Wang, H., Chen, Y., Danielpour, D., and Yang, Y. C. (2006) *Oncogene* **25,** 5547–5560
37. Bunton, T. E., Biery, N. J., Myers, L., Gayraud, B., Ramirez, F., and Dietz, H. C. (2001) *Circ. Res.* **88,** 37–43
38. Charbonneau, N. L., Ono, R. N., Corson, G. M., Keene, D. R., and Sakai, L. Y. (2004) *Birth Defects Res. C Embryo Today* **72,** 37–50
39. Brooke, B. S., Karnik, S. K., and Li, D. Y. (2003) *Trends Cell Biol.* **13,** 51–56
40. Gregory, K. E., Ono, R. N., Charbonneau, N. L., Kuo, C. L., Keene, D. R., Bächinger, H. P., and Sakai, L. Y. (2005) *J. Biol. Chem.* **280,** 27970–27980
41. Ramirez, F., and Rifkin, D. B. (2009) *Curr. Opin. Cell Biol.* **21,** 616–622
42. Massagué, J. (2008) *Mol. Cell* **29,** 149–150
43. Vollbrandt, T., Tiedemann, K., El-Hallous, E., Lin, G., Brinckmann, J., John, H., Bätge, B., Notbohm, H., and Reinhardt, D. P. (2004) *J. Biol. Chem.* **279,** 32924–32931
44. Hutchinson, S., Furger, A., Halliday, D., Judge, D. P., Jefferson, A., Dietz, H. C., Firth, H., and Handford, P. A. (2003) *Hum. Mol. Genet.* **12,** 2269–2276
45. Baldock, C., Siegler, V., Bax, D. V., Cain, S. A., Mellody, K. T., Marson, A., Haston, J. L., Berry, R., Wang, M. C., Grossmann, J. G., Roessle, M., Kielty, C. M., and Wess, T. J. (2006) *Proc. Natl. Acad. Sci. U.S.A.* **103,** 11922–11927
46. Lee, S. S., Knott, V., Jovanovi, J., Harlos, K., Grimes, J. M., Choulier, L., Mardon, H. J., Stuart, D. I., and Handford, P. A. (2004) *Structure* **12,** 717–729
47. Hubmacher, D., El-Hallous, E. I., Nelea, V., Kaartinen, M. T., Lee, E. R., and Reinhardt, D. P. (2008) *Proc. Natl. Acad. Sci. U.S.A.* **105,** 6548–6553
48. Kuo, C. L., Isogai, Z., Keene, D. R., Hazeki, N., Ono, R. N., Sengle, G., Bächinger, H. P., and Sakai, L. Y. (2007) *J. Biol. Chem.* **282,** 4007–4020
49. Sabatier, L., Chen, D., Fagotto-Kaufmann, C., Hubmacher, D., McKee, M. D., Annis, D. S., Mosher, D. F., and Reinhardt, D. P. (2009) *Mol. Biol. Cell* **20,** 846–858
50. Kinsey, R., Williamson, M. R., Chaudhry, S., Mellody, K. T., McGovern, A., Takahashi, S., Shuttleworth, C. A., and Kielty, C. M. (2008) *J. Cell Sci.* **121,** 2696–2704
51. Isogai, Z., Ono, R. N., Ushiro, S., Keene, D. R., Chen, Y., Mazzieri, R., Charbonneau, N. L., Reinhardt, D. P., Rifkin, D. B., and Sakai, L. Y. (2003) *J. Biol. Chem.* **278,** 2750–2757

OPEN ACCESS Freely available online

PLoS one

Functional Tooth Regeneration Using a Bioengineered Tooth Unit as a Mature Organ Replacement Regenerative Therapy

Masamitsu Oshima[1☯], Mitsumasa Mizuno[1,2☯], Aya Imamura[3], Miho Ogawa[1,4], Masato Yasukawa[3], Hiromichi Yamazaki[3], Ritsuko Morita[1], Etsuko Ikeda[2], Kazuhisa Nakao[1], Teruko Takano-Yamamoto[2], Shohei Kasugai[5], Masahiro Saito[1,3], Takashi Tsuji[1,3,4]*

1 Research Institute for Science and Technology, Tokyo University of Science, Noda, Chiba, Japan, **2** Division of Orthodontics and Dentofacial Orthopedics, Graduate School of Dentistry, Tohoku University, Sendai, Miyagi, Japan, **3** Department of Biological Science and Technology, Graduate School of Industrial Science and Technology, Tokyo University of Science, Noda, Chiba, Japan, **4** Organ Technologies Inc., Tokyo, Japan, **5** Oral Implantology and Regenerative Dental Medicine Graduate School, Tokyo Medical and Dental University, Bunkyo-ku, Tokyo, Japan

Abstract

Donor organ transplantation is currently an essential therapeutic approach to the replacement of a dysfunctional organ as a result of disease, injury or aging *in vivo*. Recent progress in the area of regenerative therapy has the potential to lead to bioengineered mature organ replacement in the future. In this proof of concept study, we here report a further development in this regard in which a bioengineered tooth unit comprising mature tooth, periodontal ligament and alveolar bone, was successfully transplanted into a properly-sized bony hole in the alveolar bone through bone integration by recipient bone remodeling in a murine transplantation model system. The bioengineered tooth unit restored enough the alveolar bone in a vertical direction into an extensive bone defect of murine lower jaw. Engrafted bioengineered tooth displayed physiological tooth functions such as mastication, periodontal ligament function for bone remodeling and responsiveness to noxious stimulations. This study thus represents a substantial advance and demonstrates the real potential for bioengineered mature organ replacement as a next generation regenerative therapy.

Citation: Oshima M, Mizuno M, Imamura A, Ogawa M, Yasukawa M, et al. (2011) Functional Tooth Regeneration Using a Bioengineered Tooth Unit as a Mature Organ Replacement Regenerative Therapy. PLoS ONE 6(7): e21531. doi:10.1371/journal.pone.0021531

Editor: Wei-Chun Chin, University of California, Merced, United States of America

Received April 8, 2011; **Accepted** May 30, 2011; **Published** July 12, 2011

Funding: This work was partially supported by Health and Labour Sciences Research Grants from the Ministry of Health, Labour, and Welfare (No. 21040101) to T.T., a Grant-in Aid for Scientific Research in Priority Areas (No. 50339131) to T.T., a Grant-in-Aid for Scientific Research (A) to T.T. and a Grant-in-Aid for Young Scientists (B) to M. Oshima from Ministry of Education, Culture, Sports and Technology, Japan. The funders had no role in study design, data collection and analysis, decision to publish, or preparation of the manuscript.

Competing Interests: The authors have declared that no competing interests exist.

* E-mail: t-tsuji@rs.noda.tus.ac.jp

☯ These authors contributed equally to this work.

Introduction

Donor organ transplantation is currently essential to replace a dysfunctional organ and to restore organ function *in vivo* [1,2]. This approach is problematic for clinicians however as donor organs are constantly in short supply [2,3]. An attractive new concept in current regenerative therapy that may possibly replace conventional transplantation in the future is stem cell transplantation therapy [4,5] or a two-dimensional uniform cell sheet technique [6,7] to repair the local sites of the damaged tissues and organs [8]. The ultimate goal of regenerative therapy in the future is to develop organ replacement regenerative therapies that will restore lost or damaged tissues following disease, injury, or aging with a fully functioning bioengineered organ [9,10,11]. To construct a bioengineered organ, one of two major concepts is to construct fully functional artificial organs using three-dimensional tissue-engineering technology, involving biodegradable materials and various cell types, that can immediately function after transplantation *in vivo* [12,13,14]. However, further technological developments are required to create such artificial organs which can immediately function [15].

For the regeneration of ectodermal organs such as a tooth, hair follicle or salivary gland [16,17], a further concept has been proposed in which a bioengineered organ is developed from bioengineered organ germ by reproducing the developmental processes that take place during organogenesis [11,18]. Tooth regenerative therapy is thought to be a very useful study model for organ replacement therapies [11,19,20]. The loss of a tooth causes fundamental problems in terms of oral functions, which are achieved in harmony with the teeth, masticatory muscles and the temporomandibular joint under the control of the central nervous system [21]. It has been anticipated that a bioengineered tooth could restore oral and physiological tooth functions [19]. We have previously developed a three-dimensional cell manipulation method, designated the organ germ method, for the reconstitution of bioengineered organ germ, such as a tooth or whisker follicle [22]. This bioengineered tooth erupted with the correct structure, occluded at the lost tooth region in an adult mouse. It also showed sufficient masticatory performance, periodontal functions for bone remodeling and the proper responsiveness to noxious stimulations [20]. This previous study thus provided a proof of concept that

successful replacement of an entire and fully functioning organ could be achieved through the transplantation of bioengineered organ germ i.e. a successful organ replacement regenerative therapy [20].

Transplantation of a bioengineered mature organ will lead to immediately perform of the full functions *in vivo* and have a profound impact on the survival outcomes of many diseases [2,9]. Transplanted bioengineered organs are also expected to be viable over the long-term and achieve the continuous production of various functional cells and their progenitors from stem cells as efficiently as the natural organ *in vivo* [23,24]. It has also been proposed that mature organs can be developed from bioengineered organ germ by faithfully reproducing *in vivo* developmental processes. In the dental treatment, it has been expected to transplant of a bioengineered tooth unit comprising mature tooth, periodontal ligament (PDL) and alveolar bone into the tooth loss region through bone integration, which is connected between recipient bone and bioengineered alveolar bone in a bioengineered tooth unit [25]. Transplantation of a bioengineered tooth unit has also been proposed as a viable option to repair the large resorption defects in the alveolar bone after tooth loss [26]. However, there are currently no published reports describing successful transplantation or replacement using a bioengineered tooth [10,27].

In our current study, we have generated a bioengineered tooth unit, which was controlled for length and shape and report a successful tooth replacement by transplantation of a bioengineered tooth unit into the tooth loss region, followed by successful bone integration, and restoration of tooth physiological functions such as mastication, PDL function and an appropriate responsiveness to noxious stimulations. This transplantation of a bioengineered tooth unit could also regenerate alveolar bone formation in a vertical direction. Our results thus further demonstrate the potential for bioengineered tooth replacement as a future regenerative therapy.

Results

Generation of a Bioengineered Tooth Unit

We have previously reported that bioengineered tooth germ can successfully develop a bioengineered tooth that by subrenal capsule transplantation can restore a mature tooth, including periodontal tissue and alveolar bone [22]. Because a three-dimensional *in vitro* organ culture has not yet been developed, we employed a strategy involving a bioengineered tooth unit, which has the necessary tissues to restore tooth functions, to investigation and advance the future potential of bioengineered tooth replacement (figure 1A). The bioengineered molar tooth germ was developed to a stage equivalent to the early bell stage of natural tooth germ for 5–7 days in an *in vitro* organ culture (figure 1B). Although we have previously reported that multiple bioengineered teeth have been formed from a bioengineered tooth germ reconstituted by our organ germ method [22], we recently developed a method to generate a single and width-controlled bioengineered tooth [28]. The bioengineered tooth germ gradually accumulated hard tissue, root extension, and an increased alveolar bone volume, depending on transplantation periods, and could successfully generate a tooth unit with the correct structure of a whole molar, and the proper formation of periodontal tissue and surrounding alveolar bone (figure 1C, D). However, the shape (x vs. y axis) of the bioengineered tooth unit was flattened by the pressure of the outer membrane of the subrenal capsule (figure 1F, G). The length of the tooth also showed continuous root elongation depending on the transplantation periods without occlusional mechanical stress (figure 1C, F, H).

To generate the shape- and length-controlled bioengineered tooth unit so that a suitable size was obtained for intraoral transplantation, the tooth germ was inserted into a ring-shaped size-control device and then transplanted into a subrenal capsule (figure 1E). The crown widths, calculated from the x/y axis ratios, of natural first, second and third molars of 9-week-old adult mice were 1.61±0.05 mm, 1.09±0.04 mm, 1.12±0.04 mm, respectively (each n = 5, figure 1G). The crown width of the bioengineered tooth units grown in the size-control device, which had a 1.8 mm inside diameter and 1.3 mm thickness, was 1.46±0.16 mm whereas when grown outside of the device the size was 2.30±0.35 mm (each n = 5, figure 1G). The device thus successfully generated a size-controlled bioengineered tooth so that it was similar to a natural tooth (figure 1F, G). This device could avoid the pressure by the subrenal capsule membrane, and reserve the three-dimensional space for developing a bioengineered tooth germ normally. We next evaluated the length of a bioengineered tooth unit generated in the size-control device (figure 1E). After 30 or 60 days, the lengths of the teeth transplanted without the devices were 1.07±0.20 mm and 1.70±0.26 mm, respectively, which was significantly associated with the transplantation period (each n = 5, figure 1H, figure S1A). Although the length of the bioengineered tooth transplanted without the devices was 1.70±0.26 mm after 60 days transplantation, bioengineered teeth transplanted in devices of 1.3 or 1.8 mm in diameter, was significantly regulated at 1.02±0.11 or 1.27±0.06 mm, respectively (each n = 5, figure 1H). The shape and length of the bioengineered tooth unit can therefore be controlled in three-dimensions using a specialized device.

Multiple bioengineered tooth units surrounded by alveolar bone could be also generated by the transplantation of several tooth germs into a single size-control device (figure 1I, figure S1B). Each resulting tooth had the correct structure including pulp cavities and partitioned periodontal spaces (figure 1I, figure S1C). Hence, multiple tooth replacements can be achieved with this regenerative transplantation method.

Transplantation of a Bioengineered Tooth Unit into a Tooth Loss Region *in Vivo*

We next investigated whether a bioengineered tooth unit could be engrafted via the integration between the alveolar bone of this unit and that of the host recipient and then function appropriately by occlusion with an opposing tooth (figure 2A). The bioengineered tooth unit, which was generated by transplantation in a device of a 2.5 mm inside diameter for 50–60 days and labeled by the administration of calcein reagent into recipient mouse (figure 2B), was transplanted with the correct orientation into a properly-sized bony hole in the lower first molar region of the alveolar bone in a 4-week-old mouse (figure 2C). Briefly, in this mouse model, the lower first molar had been extracted, and the resulting gingival wounds had been allowed to heal for 4–6 days (figure S2A). When the bioengineered tooth unit was transplanted, it was located at a position reaching the occlusal plane with the opposing upper first molar (figure 2C, figure S2A). Partial bone integration was observed at 14 days after transplantation, and full bone integration around a bioengineered tooth root was seen at 30 days after transplantation (figure 2C). In the calcein-labeled alveolar bone of bioengineered tooth unit, resorption was partially observed at the surface at 30 days post-transplantation (figure 2D, figure S2B). The calcein-labeled bone finally disappeared and the recipient bone around the bioengineered tooth root replaced it completely at 40 days after transplantation at a frequency of 66/83 (79.5%; figure 2C, D, figure S2B). There have been many previously reported clinical cases of multiple tooth loss, the most serious condition being edentulism [29]. It is possible that a

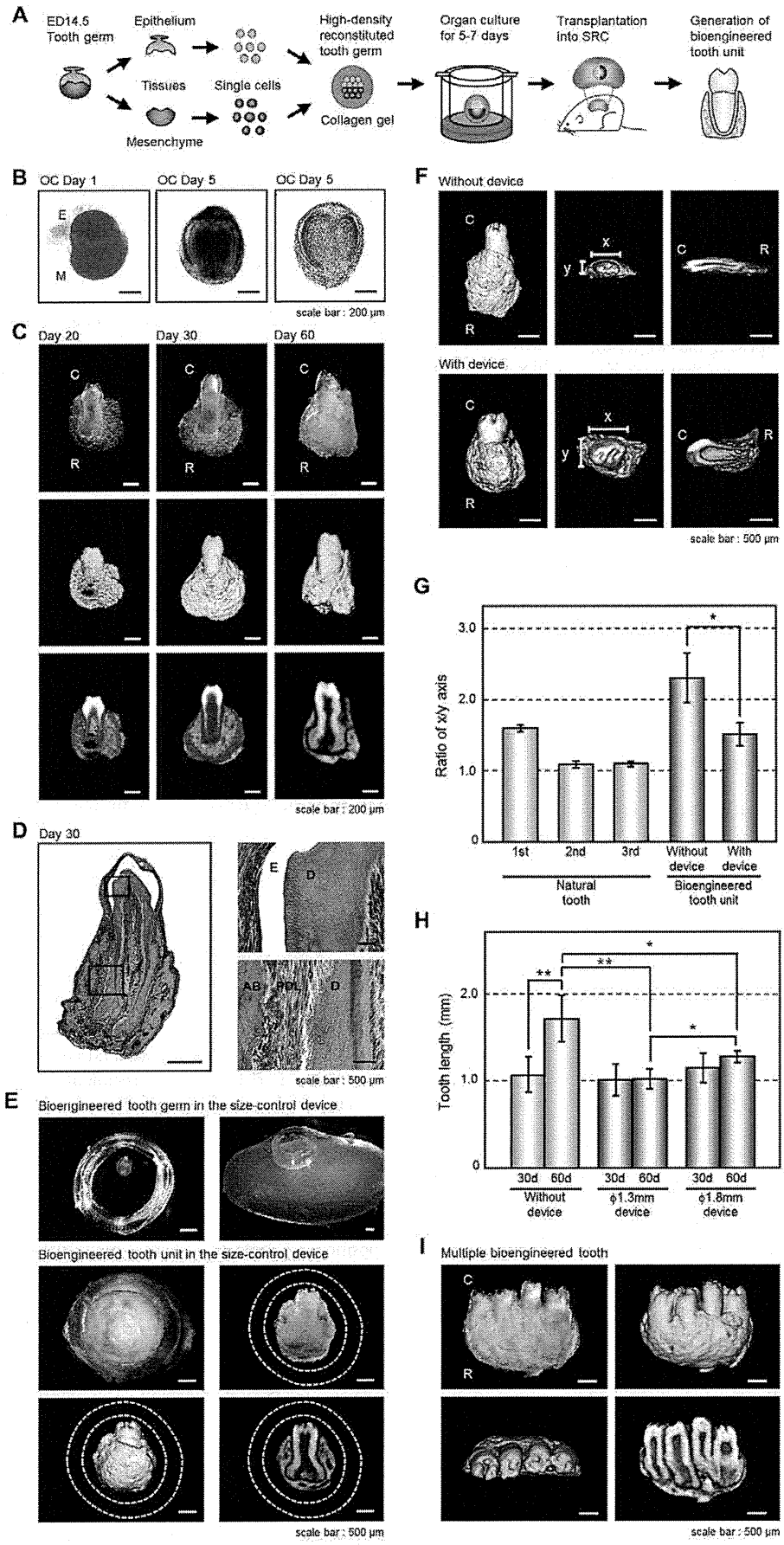
A
ED14.5 Tooth germ
Epithelium
Tissues
Single cells
Mesenchyme
High-density reconstituted tooth germ
Collagen gel
Organ culture for 5-7 days
Transplantation into SRC
Generation of bioengineered tooth unit
B
OC Day 1
OC Day 5
OC Day 5
E
M
scale bar : 200 μm
C
Day 20
Day 30
Day 60
C
R
scale bar : 200 μm
D
Day 30
E
D
AB
PDL
D
scale bar : 500 μm
E
Bioengineered tooth germ in the size-control device
Bioengineered tooth unit in the size-control device
scale bar : 500 μm
F
Without device
With device
C
R
X
y
scale bar : 500 μm
G
Ratio of xy axis
3.0
2.0
1.0
0
1st
2nd
3rd
Without device
With device
Natural tooth
Bioengineered tooth unit
H
Tooth length (mm)
2.0
1.0
0
30d
60d
Without device
φ1.3mm device
φ1.8mm device
I
Multiple bioengineered tooth
C
R
scale bar : 500 μm

Figure 1. Generation of a bioengineered tooth unit. (A) Schematic representation of the generative technology of bioengineered tooth unit. (B) Phase construct imagery of a bioengineered tooth germ on day 1 (*left*) and 5 (*center*) and HE staining (*right*) of an organ culture on day 5. Scale bar, 200 μm. E, epithelium; M, mesenchyme. (C) Photographs (*upper*) and micro-CT images of the external surface area (*middle*) and cross section (*lower*) of a bioengineered tooth unit. Images were captured at 20 days (*left*), 30 days (*center*) and 60 days (*right*) after subrenal capsule transplantation (SRC). Scale bar, 200 μm. C, tooth crown side; R, tooth root side. (D) Histological analysis of the bioengineered tooth unit on day 30 after SRC transplantation (*left*). (Scale bar, 500 μm). Higher magnification images of crown area (*upper right*) and the periodontal tissue area (*lower right*) are also shown. Scale bar, 50 μm. E, enamel; D, dentin; AB, alveolar bone; PDL, periodontal ligament. (E) Photographs of the developmental processes occurring in bioengineered tooth germ in a subrenal capsule (SRC) using a size-control device. Images were captured of bioengineered tooth germ orientated in the device (*top left*), transplantation into the SRC (*top right*), and the bioengineered tooth at 50–60 days after transplantation in the SRC (middle). Micro-CT images of the external surface area (*bottom left*) and cross section (*bottom left*) are also show. The dotted lines indicate the outlines of the device. Scale bar, 500 μm. (F) Micro-CT images of a bioengineered tooth unit transplanted into the SRC for 30 days with (*lower column*) or without (*upper column*) the size-control device at an external (*left*), axial (*center*) or cross section (*right*) view. Scale bar, 500 μm. x, x-axis of the crown; y, y-axis of the crown. (G) X-axis versus y-axis ratios (x/y) of the crowns of bioengineered tooth units at 30 days post transplantation into an SRC, and also of natural first, second and third molars from 9-week-old mice. Transplantations were performed with or without the 1.3 mm thickness size-control device. Error bars show the standard deviation ($n=5$). *$P<0.001$ (*t*-test). (H) The lengths of the bioengineered tooth units generated using size-control devices, which were of a 1.3 mm (φ1.3 mm) or 1.8 mm (φ1.8 mm) inner diameter, at 30 and 60 days post transplantation into an SRC were compared with or without the devices. Error bars show the standard deviation ($n=5$). *$P<0.01$ and **$P<0.001$ (*t*-test). (I) Photograph (*first figure from the left*) and micro-CT images showing external (*second figure*), axial (*third figure*) and cross section (*fourth figure*) views of a multiple bioengineered tooth units, in which four teeth were contained in one alveolar bone, after 60 days transplantation into the SRC. Scale bar, 500 μm.
doi:10.1371/journal.pone.0021531.g001

bioengineered teeth unit could be transplanted into an edentulous jaw (figure S2E, F). Our current findings suggest that bioengineered teeth can be engrafted into regions of tooth loss through bone integration, which involves resorption of the alveolar bone of the bioengineered tooth unit through natural bone remodeling in the recipient.

The engrafted bioengineered tooth was found to be aligned appropriately and occlude with the opposing upper first molar (figure 2E, figure S2C). Micro-CT analysis also revealed that no root elongation was evident for the bioengineered tooth and that the apical foramen of the engrafted bioengineered tooth root significantly narrowed at 40 days after transplantation (each n = 9, figure S2D). These results suggest that the bioengineered tooth in the tooth unit isolated from subrenal capsule transplantation is immature tooth, which has the potential to narrow of the apical foramen after the oral transplantation and would have the physiological ability to recapitulate mechanical stress by occlusion.

Masticatory potential is essential for proper tooth function and we next performed a Knoop hardness test, an important measure of masticatory functions, on bioengineered teeth including both the dentin and the enamel components. The Knoop hardness numbers (KHN) of the enamel and dentin in the natural teeth of 11-week-old adult mice were measured at 404.2±78.2 and 81.0±11.5, respectively (each n = 5, figure 2F). The bioengineered teeth generated in a subrenal capsule (SRC) and in jaw bone (TP) showed similar KHN values at 179.6±49.2 and 319.6±78.3 in the enamel, and 80.7±11.5 and 76.8±13.6 KHN in the dentin, respectively (each n = 5, figure 2F). The value of enamel Knoop hardness of natural tooth increase in according to postnatal period [20]. Although the enamel hardness of the bioengineered tooth generated in a SRC showed low KHN values, the enamel hardness of the engrafted bioengineered teeth (TP) increased to the high KHN value in according to the period after the transplantation into jaw bone. Therefore, the hardness of the dentin in the engrafted bioengineered teeth was in the normal range. These findings indicate that the hardness of the enamel and dentin in the engrafted bioengineered teeth were in the normal range.

Functional Analysis of the Periodontal Ligament and Neurons of the Engrafted Bioengineered Teeth

Previously, it had been demonstrated that the bioengineered tooth germ can recapitulate physiological tooth function in the adult murine oral environment [20]. In our present study, we next investigated whether an engrafted bioengineered mature tooth unit can also restore physiological tooth functions *in vivo* such as the response to mechanical stress and the perceptive potential for noxious stimulations. It is essential for tooth functions that the engrafted bioengineered tooth in recipient has the cooperation with the oral and maxillofacial regions through the PDL. The response of the PDL to mechanical stress, such as orthodontic movements, induces alveolar bone remodeling, which is indicated by the localization of tartrate-resistant acid phosphatase (TRAP)-osteoclasts and osteocalcin (*Ocn*) mRNA-positive osteoblasts [20]. During experimental tooth movement, TRAP-positive osteoclasts and *Ocn* mRNA-positive osteoblasts were observed on the compression and tension sides, respectively (figure 3A). This demonstrated that the PDL of the bioengineered tooth unit successfully mediates bone remodeling via the proper localization of osteoclasts and osteoblasts in response to mechanical stress.

The perceptive potential for noxious stimulation including mechanical stress and pain, are important for proper tooth function [30]. Trigeminal ganglional neurons, which innervate the pulp and PDL, can respond to these stimulations and transduce the perceptions to the central nervous system. Blood vessels that are detected in the pulp and PDL, maintain dental tissues such as odontoblasts, pulp, the PDL and alveolar bone. In our current experiments, we evaluated the responsiveness of nerve fibers in the pulp and PDL of the engrafted bioengineered tooth to noxious stimulations. Although von Willebrand Factor (vWF)-positive blood vessels were observed in the pulp and PDL of the bioengineered tooth generated in a subrenal capsule, anti-neurofilament (NF)-immunoreactive nerve fibers could not be detected (figure 3B, figure S3A, B). However, NF-positive nerve fibers could be detected in the pulp and PDL of the engrafted bioengineered tooth in the recipient bone and the neurons merged with vWF-positive blood vessels (figure 3B). Neuropeptide Y (NPY) and calcitonin gene-related peptide (CGRP), which are synthesized in sympathetic and sensory nerves, respectively, were also detected in both the pulp and PDL neurons (figure 3B, figure S3C–F). We found in our current analyses that c-Fos immunoreactive neurons, which are detectable in the superficial layers of the medullary dorsal horn following noxious stimulations such as mechanical and chemical stimulation of the intraoral receptive fields, were present in both normal and bioengineered teeth and drastically increased in number at two hours after orthodontic treatment and pulp exposure (figure 3C). These results indicate that an engrafted bioengineered tooth unit can indeed restore the

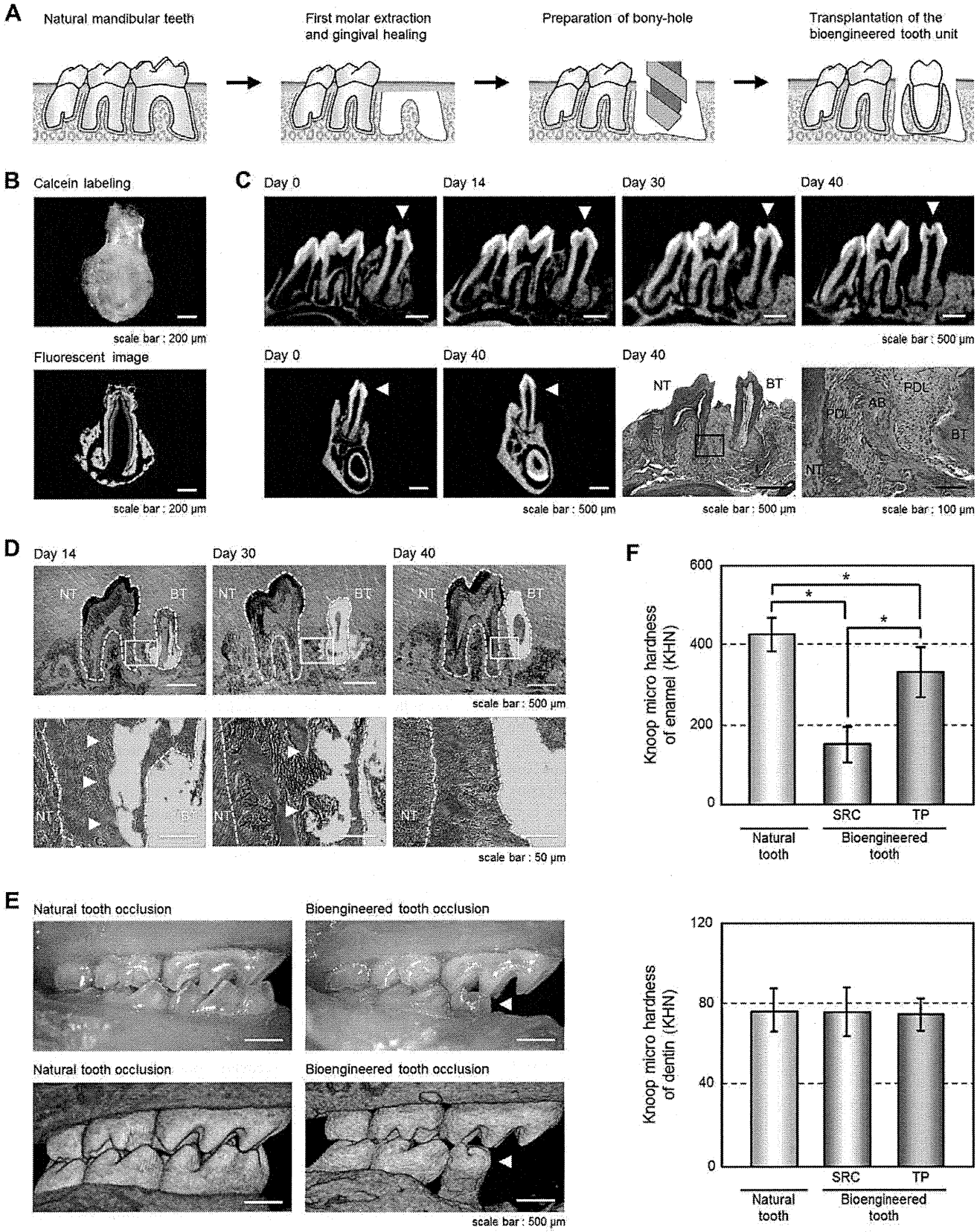

Figure 2. Engraftment and occlusion of a bioengineered tooth unit in a tooth loss model. (A) Schematic representation of the protocol used to transplant a bioengineered tooth unit in a murine tooth loss model. (B) Photograph (*Upper*) and sectional image (*Lower*) of a calcein-labeled bioengineered tooth unit at 60 days post transplantation in an SRC. Scale bar, 200 μm. (C) Micro-CT images of a bioengineered tooth unit (arrowhead) in cross section (*upper*) and frontal section (*first and second figures from the lower left*) during the processes of bone remodeling and

connection between the recipient jaw bone and alveolar bone of the tooth unit. Histological analysis of the engrafted bioengineered tooth unit at 40 days post transplantation was also performed. (Scale bar, 500 μm and 100 μm in the lower and higher magnification figure; *third and fourth figure from the lower left*). NT, natural tooth; BT, bioengineered tooth; AB, alveolar bone; PDL, periodontal ligament. (D) Sectional images of a calcein-labeled bioengineered tooth unit at 14, 30 and 40 days post-transplantation. The calcein-labeled bone of the bioengineered tooth units (arrowhead) was found to gradually decrease from the outside and finally disappear at 40 days post-transplantation. Scale bar, 500 μm (*upper*), 50 μm (*lower*). NT, natural tooth; BT, bioengineered tooth. (E) Oral photographs (*upper*) and micro-CT (*lower*) images showing occlusion of natural (*left*) and bioengineered teeth (*right*). Scale bar, 500 μm. (F) Assessment of the hardness of a bioengineered tooth. Knoop microhardness values of the enamel (*upper*) and dentin (*lower*) of a bioengineered tooth at 60 days post-transplantation in a subrenal capsule (SRC) and at 40 days post-transplantation in jawbone (TP) were compared with those of natural teeth in 11-week-old mice. Error bars show the standard deviation ($n=5$). *$P<0.01$ (*t*-test).
doi:10.1371/journal.pone.0021531.g002

perceptive potential for noxious stimulations in cooperation with the maxillofacial region.

Regeneration of an Extensive Bone Defect by Transplantation of a Bioengineered Tooth Unit

Tooth loss is well known to cause significant alveolar bone resorption at the region in question [26]. Although there have been many studies of bone regenerative therapies [31], more effective methods to restore extensive bone defects during treatments such as dental implants are required and anticipated [26]. We investigated whether the transplantation of a bioengineered tooth unit would regenerate not only the missing tooth but also the surrounding alveolar bone of the recipient. To analyze whether such restoration of the alveolar bone occurred after transplantation, we developed a murine extensive bone defect model, which was prepared by the extraction of the lower first molar and then removal of the surrounding alveolar bone to generate a critical bone defect in the lower first molar region (figure 4A, figure S4A). When we transplanted a bioengineered tooth unit into this bone defect, vertical bone formation was observed from the marginal bone of the recipient at 14 days after transplantation (figure 4B, C, figure S4B). The regenerative bone volume post-transplantation significantly increased compared with a no transplant control (0.38 ± 0.07 mm^3 vs. 0.12 ± 0.08 mm^3; each n = 4, figure 4C, D), although the height and volume of the regenerated alveolar bone surrounding the bioengineered teeth was not completely recovered. These findings indicate that transplantation of a bioengineered tooth unit can restore a serious bone defect.

Discussion

We here demonstrate the successful transplantation of a bioengineered tooth unit, which is a model for a bioengineered mature organ, into a missing tooth region *in vivo* and the subsequent restoration of tooth function by this graft. We also show that this transplantation can restore the bone volume in both the vertical and horizontal dimensions in a missing tooth mouse model with a serious extensive bone defect. These findings indicate that whole tooth regenerative therapy is feasible through the transplantation of a bioengineered mature tooth unit. This study also provides the first reported evidence of entire organ regeneration through the transplantation of a bioengineered tooth.

Organ replacement regenerative therapy, but not stem cell transplantation regenerative therapy for tissue repair, holds great promise for the future replacement of a dysfunctional organ with a bioengineered organ reconstructed using three-dimensional cell manipulation *in vitro* [11,19]. In previous reports, however, artificial organs, which were constructed with various cells and artificial materials could not restore functionality and thus are not a viable option for long-term organ replacement *in vivo* [15]. Previously, it has been shown that a bioengineered organ can be grown *in vivo* in amphibian models in which activin-treated cell aggregates could form a secondary heart with pumping function and also regenerate eyes that were light responsive and connected with the host nervous system [32,33]. Recently, we have also regenerated bioengineered organ germs, including tooth germs and whisker follicles, and successfully achieved a fully functioning tooth replacement in an adult mouse through the transplantation of a bioengineered tooth germ in the lost tooth region [20,22]. It has been anticipated that replacement therapies will be developed in the future through the transplantation of a bioengineered mature organ with full functionality and long-term viability [2,19]. In our present experiments, we successfully generated a size-controlled bioengineered mature tooth unit, a strategy we adopted because the growth of functional organs *in vitro* is not yet possible [27]. Organs require a sufficient mass (cell number) and proper shape to function [34] and the tooth has unique morphological features, such as the tooth crown width and length (macro-morphology), and cusp and root shape (micro-morphology) [35]. However, the technology to regulate tooth morphogenesis for whole tooth regeneration remains unexplored [36]. We recently developed a novel organ germ method to regulate the crown width by regulating the contact area between epithelial and mesenchymal cell layers [28]. In our previous work, we demonstrated that the length of the bioengineered tooth is equivalent to that of natural tooth after the transplantation of the bioengineered tooth germ into oral environment [20]. In this study, the length of the bioengineered tooth unit could be controlled longitudinally, which would be provided by the limited space of the device. These findings provide the first evidence that the bioengineered tooth can be controlled in three-dimensions using a specialized device. It is also thought that bioengineered teeth could be generated with a controlled crown width through cell manipulation and tooth length by placement in a size-controlling device, which places a three-dimensional spatial limitation on size [20,28].

Loss of teeth and functional disorders in the PDL or temporomandibular joint, cause fundamental problems for oral functions, such as enunciation, mastication and occlusion, and associated health issues [21]. Although, missing teeth are traditionally restored by replacement with an artificial tooth, such as a bridge, denture or osseo-integrated dental implant, it is thought that the proper restoration of tooth functions will require bone remodeling regulated by the PDL [20] and a proper responsiveness to noxious stimulations [30]. Previous reports of autologous tooth transplantations have indicated that natural periodontal tissue on the tooth could restore the physiological tooth function, including bone remodeling [37]. We recently showed that a fully functional bioengineered tooth can be achieved through the transplantation of a bioengineered organ germ [20]. In our current study, we demonstrate the successful replacement of an entire and fully functional tooth unit *in vivo*, which restored masticatory potential, the functional responsiveness, including bone remodeling, of the periodontal tissue to mechanical stress and proper responsiveness to noxious stimulations via both peripheral sensory and sympathetic nerves. This is a significant

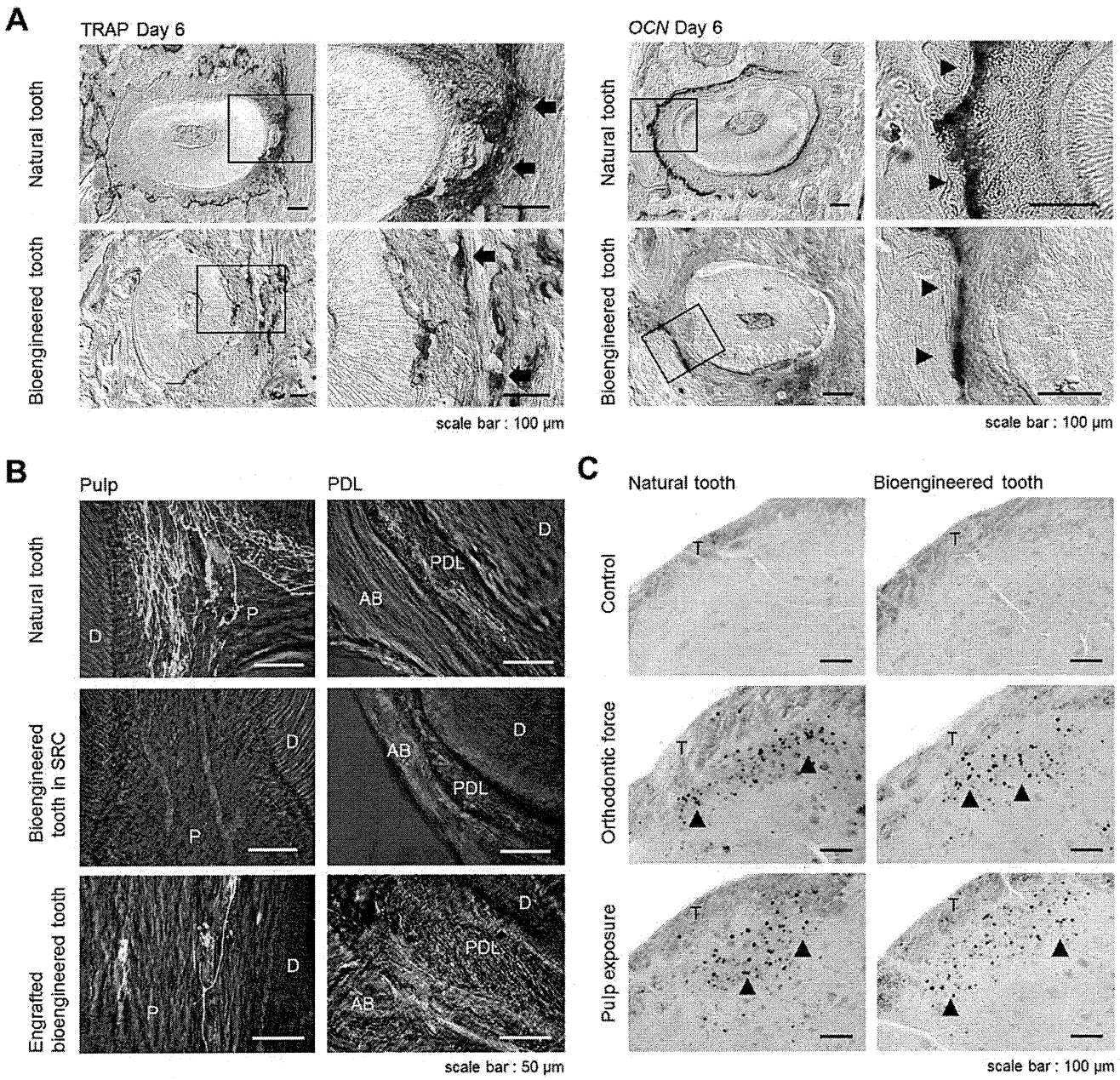

Figure 3. Experimental tooth movement and pain response to mechanical stress. (A) Sections of natural and bioengineered teeth were analyzed by TRAP-staining and *in situ* hybridization analysis of *Ocn* mRNA at day 6 of orthodontic treatment. TRAP-positive cells (arrow) and *Ocn* mRNA-positive cells (arrowhead) are indicated. Scale bar, 100 μm. (B) Nerve fibers and blood vessels in the pulp and PDL of a natural tooth (*top*), a bioengineered tooth unit in an SRC (*middle*), and a bioengineered tooth at 40 days after transplantation (*bottom*) were analyzed immunohistochemically using specific antibodies for neurofilament (NF; green) and von Willebrand Factor (vWF; red). Scale bar, 50 μm. D, dentin; P, pulp; AB, alveolar bone; PDL, periodontal ligament. (C) Analysis of c-Fos immunoreactive neurons in the medullary dorsal horns of mice after 0 hours (no stimulation, control; *top*), 2 hours of stimulation by orthodontic force (*middle*) and pulp exposure (*bottom*). C-Fos (arrowhead) was detectable after these stimulations in both natural (*left*) and bioengineered teeth at 40 days post-transplantation (*right*). Scale bar, 100 μm. T, spinal trigeminal tract.

doi:10.1371/journal.pone.0021531.g003

advance for the concept of whole tooth regenerative therapy in which the transplantation of a bioengineered mature organ, and not organ germ, can replace an organ and restore its full function.

In order for a tooth to cooperate with the maxillofacial region, it is supported by the connection between the root cementum and alveolar bone through the PDL, which has essential roles in tooth support, resorption and repair of the root cementum, and the remodeling of alveolar bone [38]. Tooth loss causes a large amount of alveolar bone resorption, which is mediated by the PDL, in the vertical and horizontal dimensions, and the loss of this bone, which leads to both functional and aesthetic problems, is difficult to rectify with standard dental therapies such as dental implant and autologous tooth transplantation [26]. Although bone regeneration has been attempted for many years through the use of tissue engineering technologies, guided bone regeneration methods, autologous bone or cell transplantation, and cytokine

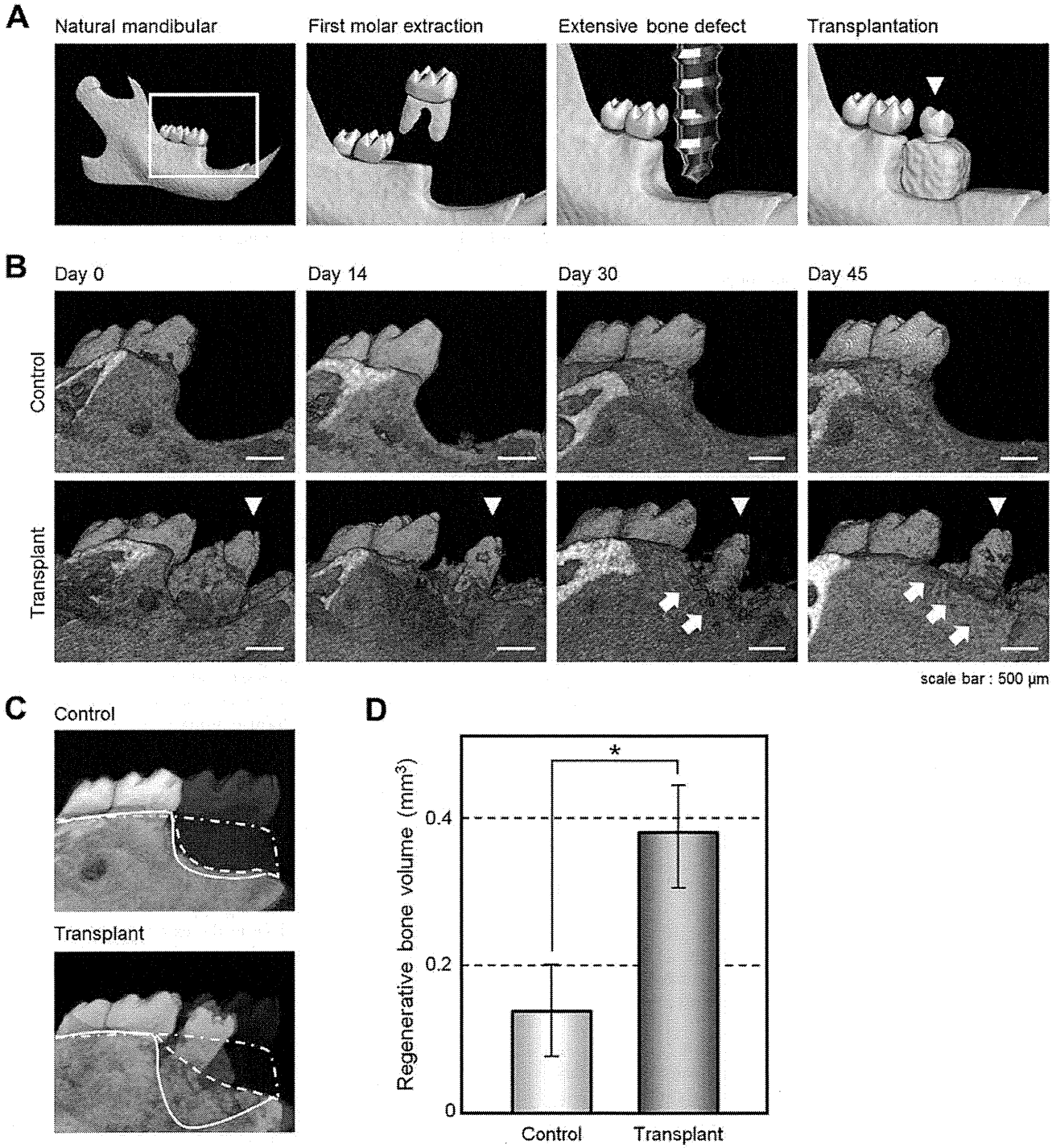

Figure 4. Alveolar bone regeneration following the transplantation of a bioengineered tooth unit. (A) Schematic representation of a murine extensive bone defect model and the transplantation of a bioengineered tooth unit (arrowhead). (B) Micro-CT images of the vertical alveolar bone regeneration processes in a no transplantation control (*upper*) and following the transplantation of a bioengineered tooth unit (arrowhead, *lower*) in a murine extensive bone defect model. Vertical bone formation was observed from the marginal bone of the recipient (arrow). Scale bar, 500 μm. (C) Three-dimensional superposition of micro-CT images of natural dentition (gray, double dotted line), a transplanted bioengineered tooth unit (*lower*) and a no transplantation control (*upper*) at day 0 in an extensive bone defect (red, straight line), and at 45 days after transplantation (green, dotted line). The superior edges of the recipient alveolar bone are indicated by each line. (D) Regenerative bone volume of the buccal area following the transplantation of a bioengineered tooth unit (transplant) and no transplantation (control) at day 45 in an extensive bone defect. Error bars show the standard deviation ($n = 4$). *$P < 0.01$ (*t*-test).
doi:10.1371/journal.pone.0021531.g004

therapies with BMPs, FGFs or PDGF, no clinical protocol for bone regeneration in the vertical and horizontal dimensions has been established yet [31]. In our present study however, we demonstrate that a bioengineered tooth unit could be engrafted and integrate via recipient bone remodeling after transplantation into an extensive bone defect. The recipient alveolar bone of the vertical dimension was observed to maintain the height of the PDL in the bioengineered tooth unit. These findings indicate that the transplantation of a bioengineered tooth has great potential for not only future whole tooth regenerative therapy but also as a treatment in clinical cases where tooth loss is accompanied by a serious alveolar bone defect.

Further studies of three-dimensional organ culture technologies *in vitro*, which can generate a fully functional bioengineered organ, and the identification of available adult tissue stem cells for the reconstitution of a bioengineered tooth germ will be required in the future to realize whole tooth regenerative therapy in the clinic.

Materials and Methods

Ethics Statement

All animals and experimental protocols were approved by the Tokyo University of Science Animal Care and Use Committee (Permit Number: N10018). All surgery was performed under sodium pentobarbital anesthesia, and all efforts were made to minimize suffering.

Reconstitution of a bioengineered tooth germ from single cells

Molar tooth germs were dissected from the mandibles of ED14.5 mice. The isolation of tissues and single cell preparations from the epithelium and mesenchyme has been described previously [22]. Dissociated epithelial and mesenchymal cells were precipitated by centrifugation in a siliconized microtube and the supernatant was completely removed. The cell density of the precipitated epithelial and mesenchymal cells after the removal of the supernatants reached a concentration of 5×10^8 cells/ml [22]. Bioengineered molar tooth germ was reconstituted using our previously described 3-dimensional cell manipulation technique, the organ germ method [22]. We used 5×10^4 epithelial and mesenchymal cells each to generate single tooth structures. The bioengineered tooth germs were incubated for 10 min at 37°C, placed on a cell culture insert (0.4 μm pore diameter; BD, Franklin Lakes, New Jersey, USA), and then further incubated at 37°C for five days in an *in vitro* organ culture as described previously [22].

Generation of a bioengineered tooth unit

To control the length and shape of the bioengineered tooth unit, we manufactured a plastic ring-shaped structure, which was used as a size-control device, of a 1.3, 1.8 or 2.5 mm inside diameter and 1.3 mm thickness. After five days of cultivation, the reconstituted tooth germs were placed into this spacing device which was transplanted into a subrenal capsule for 60 days using 7-week-old female mice as the hosts. The bioengineered tooth unit was then isolated from the device.

Fluorescent calcein labeling

Calcein (Wako, Osaka, Japan) was administered daily (1.6 mg/kg) via a subcutaneous dose to the transplanted bioengineered tooth germ in the subrenal capsule. These tooth units were then transplanted into the extracted regions of a lower first molar for 14, 30 or 40 days. Non-decalcified frozen sections were then prepared and observed using an Axiovert (Carl Zeiss, Oberkochen, Germany) with AxioCAM MRc5 (Carl Zeiss).

Transplantation

The lower first molars of 4-week-old C57BL/6 (SLC, Shizuoka, Japan) mice were extracted under deep anesthesia and the resulting gingival wounds had been allowed to heal for 4–6 days. The transplantation of a bioengineered tooth unit was allowed the procedure as described previously [20]. To generate an extensive alveolar bone defect mouse model, the whole supporting alveolar bone (1.5 mm mesiodistally, 1.2 mm buccolingually and 0.6 mm vertically) was removed using a dental engine (NSK, Tochigi, Japan) under deep anesthesia. The bioengineered tooth units were transplanted into these defects using the same procedure described above.

Microcomputed Tomography (Micro-CT)

The heads of the mice that had received a transplanted bioengineered tooth unit and normal mice were arranged in the centric occlusal position and radiographic imaging was then performed by x-ray using a Micro-CT device (R_mCT; Rigaku, Tokyo, Japan) with exposure at 90 kV and 150 mA. Micro-CT images were captured using i-view R (Morita, Kyoto, Japan) and Imaris (Carl Zeiss).

Histochemical analysis and immunohistochemistry

Histochemical and immunohistochemical tissue analyses were performed as described previously [20,22].

Hardness measurements

Polished enamel and dentin samples from bioengineered tooth units extracted at 60 days after germ transplantation into the SRC or the mandible, and also a normal tooth (9-week postnatal) were embedded in acrylic resin ($n=5$ for each group). The Knoop hardness test was then performed using a Miniload Hardness Tester (HM-102; Mitutoyo, Kanagawa, Japan) equipped with a Knoop diamond tip (19BAA061; Mitutoyo). Five indentations were made on each specimen with a 10 g load for 10 sec.

Experimental orthodontic treatments

Orthodontic treatment was performed as described previously [20]. Experimental tooth movements consisted of a horizontal orthodontic force of about 10–15 g applied continuously to the bioengineered tooth of the mice in the experimental group in a buccal direction using a dial tension gauge (Mitutoyo) for six days. In the control group, orthodontic force was applied in the buccal direction to the first molars of 7-week-old normal C57BL/6 mice in the same manner as the experimental group. Serial sections at day 6 were analyzed by TRAP staining and by *in situ* hybridization analysis for osteocalcin (*Ocn*) mRNA as previously described [20].

Pulp exposure

A minimal pinpoint mechanical exposure of the pulp was made in the bioengineered tooth or control natural first molar of mice under anesthesia using a dental engine (NSK) supplied with dental diamond point (Shofu, Kyoto, Japan). For stimulation with cold water, ice was applied to the cavity of the tooth after pulp exposure.

Measurement of the regenerative bone volume

To evaluate the extent of the alveolar bone recovery in our extensive bone defect mouse model, we used the Micro-CT device (Rigaku) to measure alveolar bone volume of the treated areas at 0 and 45 days after transplantation. We measured the volume of the alveolar bone in the operated region using TRI/3D-BON software (Ratoc, Osaka, Japan). The 3D region of interest (ROI)

was selected in the buccal alveolar bone area which was prescribed from the medial edge of lower second molar to the distal edge of the foramen mentale. We subtracted the alveolar bone volume of the area at day 0 from the volume at day 45, and calculated the regenerated bone volume.

Statistical analysis

Statistical significance was determined with the unpaired Student's *t*-test, analyzed using the Common Gateway Interface Program (twk, Saint John's University).

Supporting Information

Figure S1 A method for controlling the size of a bioengineered tooth unit. (A) Micro-CT images of the shapes of a bioengineered tooth unit, size controlled by devices of a 1.3 or 1.8 mm inner diameter, at 30 and 60 days after transplantation in an SRC. Scale bar, 500 μm. (B) Photograph of plural bioengineered tooth germ arranged in a size controlled device. Scale bar, 500 μm. (C) Micro-CT images (*left*) and histological analysis of the multiple bioengineered tooth units on day 60 after SRC transplantation (*middle and right*). The alveolar bone between the bioengineered teeth is indicated by arrowheads (*lower left*). Scale bar, 200 μm. Higher magnification images of the periodontal tissue area (*lower middle and right*) are also shown. Scale bar, 50 μm. D, dentin; AB, alveolar bone; PDL, periodontal ligament.
(TIF)

Figure S2 Engraftment and establishment of occlusion of a bioengineered tooth unit at the tooth loss region. (A) Oral photographs and micro-CT images of bioengineered tooth unit transplantations into the adult mandible. Images were captured of lateral (*top*), occlusal (*middle*) and cross sections (*bottom*) views. The bioengineered tooth unit is indicated by an arrowhead. Scale bar, 500 μm. (B) Sectional images of a calcein-labeled bioengineered tooth unit at 14, 30 and 40 days after transplantation into a murine model. Fluorescent and DIC images are merged. The alveolar bone of the bioengineered tooth unit is indicated by arrowheads. Scale bar, 500 μm, *upper*; 100 μm, *lower*. NT, natural tooth; BT, bioengineered tooth. (C) Oral photographs of an engrafted bioengineered tooth in a lateral view (upper left), a 45-degree view (*lower left*), an occlusal view (*upper right*) and a fluorescent image (*lower right*). Scale bar, 500 μm. (D) Measurements of the tooth length (*left*) and apical foramen width (*right*) of a bioengineered tooth at day 0 and day 40 after transplantation. Error bars show the standard deviation ($n = 9$). *$P<0.05$ (*t*-test). (E) Schematic representation of the protocol for transplanting multiple bioengineered tooth units in a murine edentulous model. (F) Micro-CT images of transplanted multiple bioengineered tooth units in a murine edentulous model. Images were captured of the external surface area (*left*), sagittal section (*center*) and cross section (*right*). The bioengineered teeth are indicated by the arrowheads in *the left figure*. Scale bar, 500 μm.
(TIF)

Figure S3 Regeneration of nerve fibers and blood vessels in the engrafted bioengineered tooth unit. (A, B) Nerve fibers and blood vessels in the pulp (A) and PDL (B) of a natural tooth (*top*), bioengineered tooth unit in an SRC (*middle*) and bioengineered tooth at 40 days after transplantation into an oral tooth loss region (*bottom*) were analyzed immunohistochemically using specific antibodies for NF and vWF. DIC (*first columns from the left*), NF images (*second columns*), vWF images (*third columns*), and merged images (*fourth columns*) are shown. Scale bar, 50 μm. (C, D) Nerve fibers in the pulp (C) and PDL (D) of a natural tooth (*top*), bioengineered tooth unit in an SRC (*middle*) and bioengineered tooth at 40 days after transplantation (*bottom*) were analyzed immunohistochemically using specific antibodies for NF and neuropeptide Y (NPY). DIC (*first columns from the left*), NF images (*second columns*), NPY images (*third columns*), and merged images (*fourth columns*) are shown. Scale bar, 50 μm. (E, F) Nerve fibers in the pulp (E) and PDL (F) of a natural tooth (*top*), bioengineered tooth unit in an SRC (*middle*) and bioengineered tooth at 40 days after transplantation (*bottom*) were analyzed immunohistochemically using specific antibodies for NF and calcitonin gene-related peptide (CGRP). DIC (*first columns from the left*), NF images (*second columns*), CGRP images (*third columns*), and merged images (*fourth columns*) are shown. Scale bar, 50 μm.
(TIF)

Figure S4 Alveolar bone regenerative potential of a bioengineered tooth unit. (A) Photographs of a lateral (*left*) and occlusal (*right*) view of a natural mandibular dentition and an extensive bone defect (arrowhead). Scale bar, 500 μm. (B) Micro-CT images of the frontal section of a no transplantation control (*upper*) and a transplanted bioengineered tooth unit at day 45 in a murine extensive bone defect model (*lower*). Significant vertical bone regeneration was observed following the transplantation of a bioengineered tooth unit when compared with the no transplantation control. The regenerated alveolar bone is indicated by an arrow. Scale bar, 500 μm.
(TIF)

Author Contributions

Performed the experiments: M. Oshima MM MY KN. Analyzed the data: AI M. Ogawa HY. Wrote the paper: M. Oshima TT. Designed the research plan: TT M. Oshima. Developed new assay systems and the discussion of the results: M. Ogawa RM EI TT-Y SK MS.

References

1. Lechler RI, Sykes M, Thomson AW, Turka LA (2005) Organ transplantation–how much of the promise has been realized? Nat Med 11: 605–613.
2. Gridelli B, Remuzzi G (2000) Strategies for making more organs available for transplantation. N Engl J Med 343: 404–410.
3. Moers C, Smits JM, Maathuis MH, Treckmann J, van Gelder F, et al. (2009) Machine perfusion or cold storage in deceased-donor kidney transplantation. N Engl J Med 360: 7–19.
4. Copelan EA (2006) Hematopoietic stem-cell transplantation. N Engl J Med 354: 1813–1826.
5. Nishikawa S, Goldstein RA, Nierras CR (2008) The promise of human induced pluripotent stem cells for research and therapy. Nat Rev Mol Cell Biol 9: 725–729.
6. Miyahara Y, Nagaya N, Kataoka M, Yanagawa B, Tanaka K, et al. (2006) Monolayered mesenchymal stem cells repair scarred myocardium after myocardial infarction. Nat Med 12: 459–465.
7. Ohashi K, Yokoyama T, Yamato M, Kuge H, Kanehiro H, et al. (2007) Engineering functional two- and three-dimensional liver systems in vivo using hepatic tissue sheets. Nat Med 13: 880–885.
8. Korbling M, Estrov Z (2003) Adult stem cells for tissue repair - a new therapeutic concept? N Engl J Med 349: 570–582.
9. Atala A (2005) Tissue engineering, stem cells and cloning: current concepts and changing trends. Expert Opin Biol Ther 5: 879–892.
10. Purnell B (2008) New release: the complete guide to organ repair. Introduction Science 322: 1489.
11. Ikeda E, Tsuji T (2008) Growing bioengineered teeth from single cells: potential for dental regenerative medicine. Expert Opin Biol Ther 8: 735–744.
12. Layer PG, Robitzki A, Rothermel A, Willbold E (2002) Of layers and spheres: the reaggregate approach in tissue engineering. Trends Neurosci 25: 131–134.
13. Yelick PC, Vacanti JP (2006) Bioengineered teeth from tooth bud cells. Dent Clin North Am 50: 191–203, viii.
14. Khademhosseini A, Langer R, Borenstein J, Vacanti JP (2006) Microscale technologies for tissue engineering and biology. Proc Natl Acad Sci U S A 103: 2480–2487.
15. Uygun BE, Soto-Gutierrez A, Yagi H, Izamis ML, Guzzardi MA, et al. (2010) Organ reengineering through development of a transplantable recellularized liver graft using decellularized liver matrix. Nat Med 16: 814–820.

16. Zheng Y, Du X, Wang W, Boucher M, Parimoo S, et al. (2005) Organogenesis from dissociated cells: generation of mature cycling hair follicles from skin-derived cells. J Invest Dermatol 124: 867–876.
17. Shackleton M, Vaillant F, Simpson KJ, Stingl J, Smyth GK, et al. (2006) Generation of a functional mammary gland from a single stem cell. Nature 439: 84–88.
18. Yen AH, Sharpe PT (2006) Regeneration of teeth using stem cell-based tissue engineering. Expert Opin Biol Ther 6: 9–16.
19. Sharpe PT, Young CS (2005) Test-tube teeth. Sci Am 293: 34–41.
20. Ikeda E, Morita R, Nakao K, Ishida K, Nakamura T, et al. (2009) Fully functional bioengineered tooth replacement as an organ replacement therapy. Proc Natl Acad Sci U S A 106: 13475–13480.
21. Nickel JC, Iwasaki LR, Walker RD, McLachlan KR, McCall WD, Jr. (2003) Human masticatory muscle forces during static biting. J Dent Res 82: 212–217.
22. Nakao K, Morita R, Saji Y, Ishida K, Tomita Y, et al. (2007) The development of a bioengineered organ germ method. Nat Methods 4: 227–230.
23. Zaret KS, Grompe M (2008) Generation and regeneration of cells of the liver and pancreas. Science 322: 1490–1494.
24. Slack JM (2008) Origin of stem cells in organogenesis. Science 322: 1498–1501.
25. Hu B, Nadiri A, Kuchler-Bopp S, Perrin-Schmitt F, Peters H, et al. (2006) Tissue engineering of tooth crown, root, and periodontium. Tissue Eng 12: 2069–2075.
26. Van der Weijden F, Dell'Acqua F, Slot DE (2009) Alveolar bone dimensional changes of post-extraction sockets in humans: a systematic review. J Clin Periodontol 36: 1048–1058.
27. Wang X, Yan Y, Zhang R (2010) Recent trends and challenges in complex organ manufacturing. Tissue Eng Part B Rev 16: 189–197.
28. Ishida K, Murofushi M, Nakao K, Morita R, Ogawa M, et al. (2011) The regulation of tooth morphogenesis is associated with epithelial cell proliferation and the expression of Sonic hedgehog through epithelial-mesenchymal interactions. Biochem Biophys Res Commun 405: 455–461.
29. Geertman ME, Slagter AP, van Waas MA, Kalk W (1994) Comminution of food with mandibular implant-retained overdentures. J Dent Res 73: 1858–1864.
30. Byers MR, Narhi MV (1999) Dental injury models: experimental tools for understanding neuroinflammatory interactions and polymodal nociceptor functions. Crit Rev Oral Biol Med 10: 4–39.
31. Bueno EM, Glowacki J (2009) Cell-free and cell-based approaches for bone regeneration. Nat Rev Rheumatol 5: 685–697.
32. Kinoshita M, Ariizumi T, Yuasa S, Miyoshi S, Komazaki S, et al. (2010) Creating frog heart as an organ: in vitro-induced heart functions as a circulatory organ in vivo. Int J Dev Biol 54: 851–856.
33. Sedohara A, Komazaki S, Asashima M (2003) In vitro induction and transplantation of eye during early Xenopus development. Dev Growth Differ 45: 463–471.
34. Tyler D, Baker NE (2003) Size isn't everything. Bioessays 25: 5–8.
35. Cai J, Cho SW, Kim JY, Lee MJ, Cha YG, et al. (2007) Patterning the size and number of tooth and its cusps. Dev Biol 304: 499–507.
36. Jernvall J, Thesleff I (2000) Reiterative signaling and patterning during mammalian tooth morphogenesis. Mech Dev 92: 19–29.
37. Kallu R, Vinckier F, Politis C, Mwalili S, Willems G (2005) Tooth transplantations: a descriptive retrospective study. Int J Oral Maxillofac Surg 34: 745–755.
38. Cho MI, Garant PR (2000) Development and general structure of the periodontium. Periodontol 2000 24: 9–27.

Received: Nov. 8, 2011
Accepted: Jan. 24, 2012
Published online: Feb. 29, 2012

Review Article

Dental Regenerative Therapy using Oral Tissues

Narisato Kanamura [1)], Takeshi Amemiya [1)], Toshiro Yamamoto [1)], Kenji Mishima [2)], Masahiro Saito [3,4)], Takashi Tsuji [3,4,5)], Takahiro Nakamura [6,7)]

1) Dental Medicine, Graduate School of Medical Science, Kyoto Prefectural University of Medicine
2) Department of Pathology, Tsurumi University School of Dental Medicine (Current affiliation: Department of Oral Pathology, Showa University Dental School)
3) Research Institute for Science and Technology, Tokyo University of Science
4) Department of Biological Science and Technology, Graduate School of Industrial Science and Technology, Tokyo University of Science
5) Organ Technologies Inc.
6) Research Center for Inflammation and Regenerative Medicine, Faculty of Life and Medical Sciences, Doshisha University
7) Department of Ophthalmology, Kyoto Prefectural University of Medicine

Abstract

Anti-Aging Medicine is a theoretical and practical science which aims to ensure the achievement of a long and healthy life. Dental medicine plays an important role in its practice. Given the substantial influence of dental/oral diseases on general health, the maintenance and improvement of oral function promotes not only dental/oral Anti-Aging but also systemic Anti-Aging as well.

The current target of Anti-Aging dental medicine is the prevention or slowing down of the age-related decline in oral function by evaluating indicators of oral function, such as dental age, periodontal age, occlusion age, swallowing age, and salivary age. In this symposium, Dr. Kenji Mishima (Department of Dentistry, Tsurumi University), speaking on "Application of Cell Transplantation Therapy to Salivary Gland Dysfunction", Dr. Masahiro Saito (Research Institute for Science and Technology, Tokyo University of Science), speaking on "Role of Tooth Regeneration in Anti-Aging Medicine" and myself, Dr. Narisato Kanemura (Dental Medicine, Graduate School of Medical Science, Kyoto Prefectural University of Medicine), speaking on "Development of a New Periodontal Tissue Regeneration Method Aimed at Anti-Aging Use", delivered presentations about the current status and future prospects of regenerative dentistry, which aims not only to prevent a decrease in oral function but also to restore it when function is lost, and introduced the latest in regenerative dentistry involving the salivary glands, teeth, oral mucosal epithelia, and periodontal ligaments. In addition, to describe collaboration between dental medicine and ophthalmology, Dr. Takahiro Nakamura (Faculty of Life and Medical Sciences, Doshisha University), speaking on "Current Status and Future Prospects of Corneal Regenerative Therapy using Oral Tissue", introduced the current status and future prospects of corneal regenerative therapy using periodontal mucosal epithelium. Summaries of these lectures are presented here. In the "Dental Regenerative Therapy using Oral Tissues" symposium at the 2011 11th Scientific Meeting of the Japanese Society of Anti-Aging Medicine, the experts were invited to report recent findings on maintenance.

KEY WORDS: oral tissue, regenerative therapy, saliva, tooth regenerative therapy, periodontal ligament

1. Application of Cell Transplantation Therapy to Salivary Gland Dysfunction

The causes of salivary gland dysfunction include refractory diseases such as Sjogren's syndrome and Stevens-Johnson syndrome, radiation therapy against head and neck cancer, and a variety of drugs [1)]. Current treatments include the use of artificial saliva and oral therapy with muscarinic acetylcholine receptor agonists, which stimulate salivary secretion from residual acinar cells. Severe cases may be resistant to these treatments, and patients may develop oral cavity lesions such as mucositis, caries, or periodontal disease. In addition, as salivary gland dysfunction is a pathogenic factor in aspiration pneumonia in the elderly, serious concerns have been expressed about infection treatment methods. The possibilities of regenerative medicine have therefore been investigated, specifically the reconstruction of lost gland tissues using transplantation of exogenous salivary gland stem cells. However, cell surface markers specific to salivary gland stem cells are difficult to isolate and thus remain unknown. We have therefore focused on a cell population called "side population (SP)" cells, which can be isolated without using a cell surface marker. Since their first isolation from bone marrow as a fraction containing a high frequency of stem cells, SP cells have been analyzed in a variety of organs [2-6)]. In the present study, we investigated the effects of experimental treatment with SP cells using a mouse model of irradiation-induced salivary gland dysfunction, and the possibility of establishing a treatment approach with a specific factor expressed in SP cells.

Narisato Kanamura
Dental Medicine, Graduate School of Medical Science, Kyoto Prefectural University of Medicine
Kajii-cho 465, Kawaramachi-Hirokoji, Kamigyo-ku, Kyoto 602-8566, Japan
Tel & Fax: +81-75-251-5641 / E-mail: kanamura@koto.kpu-m.ac.jp